

ISSN : 2165-4069(Online)

ISSN : 2165-4050(Print)



IJARAI

International Journal of  
Advanced Research in Artificial Intelligence

Volume 2 Issue 10

[www.ijarai.thesai.org](http://www.ijarai.thesai.org)

A Publication of  
The Science and Information Organization



INTERNATIONAL JOURNAL OF  
ADVANCED RESEARCH IN ARTIFICIAL INTELLIGENCE



THE SCIENCE AND INFORMATION ORGANIZATION  
[www.thesai.org](http://www.thesai.org) | [info@thesai.org](mailto:info@thesai.org)



# Editorial Preface

## *From the Desk of Managing Editor...*

"The question of whether computers can think is like the question of whether submarines can swim." — Edsger W. Dijkstra, the quote explains the power of Artificial Intelligence in computers with the changing landscape. The renaissance stimulated by the field of Artificial Intelligence is generating multiple formats and channels of creativity and innovation.

This journal is a special track on Artificial Intelligence by The Science and Information Organization and aims to be a leading forum for engineers, researchers and practitioners throughout the world.

The journal reports results achieved; proposals for new ways of looking at AI problems and include demonstrations of effectiveness. Papers describing existing technologies or algorithms integrating multiple systems are welcomed. IJARAI also invites papers on real life applications, which should describe the current scenarios, proposed solution, emphasize its novelty, and present an in-depth evaluation of the AI techniques being exploited. IJARAI focusses on quality and relevance in its publications.

In addition, IJARAI recognizes the importance of international influences on Artificial Intelligence and seeks international input in all aspects of the journal, including content, authorship of papers, readership, paper reviewers, and Editorial Board membership.

The success of authors and the journal is interdependent. While the Journal is in its initial phase, it is not only the Editor whose work is crucial to producing the journal. The editorial board members, the peer reviewers, scholars around the world who assess submissions, students, and institutions who generously give their expertise in factors small and large— their constant encouragement has helped a lot in the progress of the journal and shall help in future to earn credibility amongst all the reader members.

I add a personal thanks to the whole team that has catalysed so much, and I wish everyone who has been connected with the Journal the very best for the future.

**Thank you for Sharing Wisdom!**

**Managing Editor**  
**IJARAI**  
**Volume 2 Issue 10 October 2013**  
**ISSN: 2165-4069(Online)**  
**ISSN: 2165-4050(Print)**  
**©2013 The Science and Information (SAI) Organization**

# Editorial Board

**Peter Sapaty - Editor-in-Chief**

**National Academy of Sciences of Ukraine**

Domains of Research: Artificial Intelligence

**Alaa F. Sheta**

**Electronics Research Institute (ERI)**

Domain of Research: Evolutionary Computation, System Identification, Automation and Control, Artificial Neural Networks, Fuzzy Logic, Image Processing, Software Reliability, Software Cost Estimation, Swarm Intelligence, Robotics

**Antonio Dourado**

**University of Coimbra**

Domain of Research: Computational Intelligence, Signal Processing, data mining for medical and industrial applications, and intelligent control.

**David M W Powers**

**Flinders University**

Domain of Research: Language Learning, Cognitive Science and Evolutionary Robotics, Unsupervised Learning, Evaluation, Human Factors, Natural Language Learning, Computational Psycholinguistics, Cognitive Neuroscience, Brain Computer Interface, Sensor Fusion, Model Fusion, Ensembles and Stacking, Self-organization of Ontologies, Sensory-Motor Perception and Reactivity, Feature Selection, Dimension Reduction, Information Retrieval, Information Visualization, Embodied Conversational Agents

**Liming Luke Chen**

**University of Ulster**

Domain of Research: Semantic and knowledge technologies, Artificial Intelligence

**T. V. Prasad**

**Lingaya's University**

Domain of Research: Bioinformatics, Natural Language Processing, Image Processing, Robotics, Knowledge Representation

**Wichian Sittiprapaporn**

**Maharakham University**

Domain of Research: Cognitive Neuroscience; Cognitive Science

**Yaxin Bi**

**University of Ulster**

Domains of Research: Ensemble Learning/Machine Learning, Multiple Classification Systems, Evidence Theory, Text Analytics and Sentiment Analysis

---

## Reviewer Board Members

- **AKRAM BELGHITH**  
University Of California, San Diego
- **ALAA F. SHETA**  
Electronics Research Institute (ERI)
- **ALBERT ALEXANDER**  
Kongu Engineering College
- **ALPA KALPESH RESHAMWALA**  
NMIMS, MPSTME
- **AMIR HAJJAM EL HASSANI**  
Université de Technologie de Belfort-Monbéliard
- **AMIT VERMA**  
Department in Rayat & Bahra Engineering College, Mo
- **AMITAVA BISWAS**  
Cisco Systems
- **ANTONIO DOURADO**  
University of Coimbra
- **ASIM TOKGOZ**  
Marmara University
- **B R SARATH KUMAR**  
LENORA COLLEGE OF ENGINEERING
- **BABATUNDE OPEOLUWA AKINKUNMI**  
University of Ibadan
- **BESTOUN S.AHMED**  
Universiti Sains Malaysia
- **BHANU PRASAD PINNAMANENI**  
Rajalakshmi Engineering College; Matrix Vision GmbH
- **CHIEN-PENG HO**  
Information and Communications Research Laboratories, Industrial Technology Research Institute of Taiwan
- **DAVID M W POWERS**  
Flinders University
- **DIMITRIS CHRYSOSTOMOU**  
Production and Management Engineering / Democritus University of Thrace
- **EHSAN MOHEBI**  
University of Ballarat
- **FABIO MERCORIO**  
University of Milan-Bicocca
- **FRANCESCO PERROTTA**  
University of Macerata
- **FRANK IBIKUNLE**  
Covenant University
- **GERARD DUMANCAS**  
Oklahoma Medical Research Foundation
- **GORAKSH GARJE**  
Pune Vidyarthi Griha's College of Engineering and Technology, Pune
- **GRIGORAS GHEORGHE**  
"Gheorghe Asachi" Technical University of Iasi, Romania
- **GUANDONG XU**  
Victoria University
- **HAIBO YU**  
Shanghai Jiao Tong University
- **HARCO LESLIE HENDRIC SPITS WARNARS**  
Budi Luhur university
- **IBRAHIM ADEPOJU ADEYANJU**  
Ladoke Akintola University of Technology, Ogbomoso, Nigeria
- **IMRAN CHAUDHRY**  
National University of Sciences & Technology, Islamabad
- **JABAR H YOUSIF**  
Faculty of computing and Information Technology, Sohar University, Oman
- **JATINDERKUMAR R. SAINI**  
S.P.College of Engineering, Gujarat
- **JOSÉ SANTOS REYES**  
University of A Coruña (Spain)
- **KRASIMIR YORDZHEV**  
South-West University, Faculty of Mathematics and Natural Sciences, Blagoevgrad, Bulgaria
- **KRISHNA PRASAD MIYAPURAM**  
University of Trento
- **LIMING LUKE CHEN**  
University of Ulster
- **M. REZA MASHINCHI**
- **MALACK OTERI**  
jkuat
- **MAREK REFORMAT**  
University of Alberta
- **MD. ZIA UR RAHMAN**  
Narasaraopeta Engg. College, Narasaraopeta

- **MOHAMED NAJEH LAKHOVA**  
ESTI, University of Carthage
- **MOKHTAR BELDJEHEM**  
University of Ottawa
- **MONJI KHERALLAH**  
University of Sfax
- **PARMINDER SINGH KANG**  
De Montfort University, Leicester, UK
- **PETER SAPATY**  
National Academy of Sciences of Ukraine
- **PRASUN CHAKRABARTI**  
Sir Padampat Singhanian University
- **QIFENG QIAO**  
University of Virginia
- **RAJESH KUMAR**  
National University of Singapore
- **RASHAD AL-JAWFI**  
Ibb University
- **REZA FAZEL-REZAI**  
Electrical Engineering Department,  
University of North Dakota
- **SAID GHONIEMY**  
Taif University
- **SAMARJEET BORAH**  
Dept. of CSE, Sikkim Manipal University
- **SAURABH PAL**  
VBS Purvanchal University, Jaunpur
- **SECUI DINU CALIN**  
IEEE Membership; IEEE Power & Energy  
Society Membership; IEEE Computational  
Intelligence Society Membership
- **SHAHABODDIN SHAMSHIRBAND**  
University of Malaya
- **SHRINIVAS PRABHAKARRAO DESHPANDE**
- **SIMON EWEDAFE**  
Baze University
- **SUKUMAR SENTHILKUMAR**  
Universiti Sains Malaysia
- **T C.MANJUNATH**  
HKBK College of Engg
- **T V NARAYANA RAO**  
Hyderabad Institute of Technology and  
Management
- **T. V. PRASAD**  
Lingaya's University
- **V BABY DEEPA**
- **VIJAY JHA**  
BIT MESRA, Ranchi (Jharkhand)
- **VISHAL GOYAL**
- **VITUS S.W. LAM**
- **VUDA SREENIVASARAO**  
St. Mary's College of Engineering &  
Technology
- **WEI ZHONG**  
University of south Carolina Upstate
- **WICHIAN SITIPRAPAPORN**  
Mahasarakham University
- **YAXIN BI**  
University of Ulster
- **YUVAL COHEN**  
The Open University of Israel
- **ZHAO ZHANG**  
Deptment of EE, City University of Hong  
Kong
- **ZHIGANG YIN**  
Institute of Linguistics, Chinese Academy of  
Social Sciences
- **ZNE-JUNG LEE**  
Dept. of Information management, Huafan  
University

# CONTENTS

**Paper 1: Cheap and Effective System for Parking Avoidance of the Car Without Permission at Disabled Parking Permit Spaces**

*Authors: Kohei Arai*

**PAGE 1 – 6**

**Paper 2: Noise Suppressing Edge Enhancement Based on Genetic Algorithm Taking Into Account Complexity of Target Images Measured with Fractal Dimension**

*Authors: Kohei Arai*

**PAGE 7 – 13**

**Paper 3: Comparison Among Cross, Onboard and Vicarious Calibrations for Terra/ASTER/VNIR**

*Authors: Kohei Arai*

**PAGE 14 – 18**

**Paper 4: Image Retrieval and Classification Method Based on Euclidian Distance Between Normalized Features Including Wavelet Descriptor**

*Authors: Kohei Arai*

**PAGE 19 – 25**

**Paper 5: Numerical Representation of Web Sites of Remote Sensing Satellite Data Providers and Its Application to Knowledge Based Information Retrievals with Natural Language**

*Authors: Kohei Arai*

**PAGE 26 – 31**

# Cheap and Effective System for Parking Avoidance of the Car Without Permission at Disabled Parking Permit Spaces

Kohei Arai<sup>1</sup>

Graduate School of Science and Engineering  
Saga University  
Saga City, Japan

**Abstract**—Cheap and effective system for parking avoidance of the car without permission at Disabled Parking Permit: DPP spaces is proposed. The proposed system is validated through some experiments. Multiple methods for detection of car in the DPP space using ultrasound sensors, Near Infrared: NIR cameras, RFID writer and reader with IC card, IC chip and IC tag as well as ETC system and GPS receiver are proposed. It is found that these proposed car detection systems work well. Furthermore, it is effective if more than two systems out of the proposed car detection systems are used for avoid car parking without permission.

**Keywords**—Disabled Parking Permit; ultrasound sensor; Near Infrared cameras; RFID writer and reader with IC card; IC chip and IC tag; ETC system; GPS receiver

## I. INTRODUCTION

A disabled parking permit is known as a handicapped permit, disabled placard, disabled badge and "Blue Badge" in the European Union: EU under the Chronically Sick and Disabled Persons Act which was established in 1970<sup>1</sup>. The blue badge is displayed upon parking a vehicle carrying a person whose mobility would be otherwise significantly impaired by one or more of age, illness, disability or infirmity. Since 2000, all general disabled parking permits in the European Union: EU have been standardized to a common style and blue color, leading to the officially-used designation "Blue Badge".

In Ireland, Disabled Persons' Parking Permits: DPPP are issued by the Disabled Drivers Association of Ireland while United Kingdom provided a service that covers country wide customized maps for Blue Badge Holders with different base colors reflecting council's policies on Blue Badge Holder's parking<sup>2</sup>. The standard scheme only generally applies to on-street parking and is outlined on the Roads Service Northern Ireland website<sup>3</sup>.

In the United States, reserved spaces are mandated by the Americans with Disabilities Act Accessibility Guidelines<sup>4</sup>: 26 states adopted Disability Parking Permit: DPP systems. Four states include deafness, and only two states (Virginia and New

York) include mental illness or developmental disabilities. Parking spaces reserved for the disabled are typically marked with the International Symbol of Access: ISA, though in practice, the design of the symbol varies widely. If traveling from other countries, requirements to obtain a parking permit vary from state to state. Some states will honor other country permits, while others require application as a visitor/tourist.

Parking for the handicapped driver in New York City is limited to those with New York City-issued handicapped placards<sup>5</sup>. No other handicap placards are recognized as valid. In 1997 a woman with multiple sclerosis using a wheelchair was similarly issued a ticket while parking in New York City for displaying a non-NYC issued handicap placard. The abuse and/or misuse of disabled parking permits has been identified as a major problem in the US, with some estimates indicating the majority seen on the street are used or obtained fraudulently. Disabled persons who hold parking permits but have invisible disabilities may be difficult to tell apart from fraudulent permit users. Some conditions which make a disabled parking permit necessary are invisible without medical training. An injury or illness which causes an individual to be unable to walk very far may not be obvious, and a prosthesis or healing injury may be hidden under clothing. On occasion, suspicion of fraud has led to hostility against legitimate permit holders.

In Australia, disabled parking permits are provided under the Australian Disability Parking Scheme, which was established in September 2010 to harmonize disability permits across Australia<sup>6</sup>. Disabled parking permits are applied for through state and territory organizations, and rules for eligibility differ among jurisdictions.

In Japan, Saga prefectural government started DPP system in 2006<sup>7</sup>. They provide DPP for more than 10 thousand disabled persons, pregnant, elderly peoples, etc. DPP is just for disabled persons while DPP Plus One: DPPPO system

<sup>5</sup> [http://www.nyc.gov/html/dot/html/permits/pppinfo.shtml#nyc\\_permit](http://www.nyc.gov/html/dot/html/permits/pppinfo.shtml#nyc_permit)

<sup>6</sup> <http://www.disabilityparking.gov.au/>

<sup>7</sup> [http://www.pref.saga.lg.jp/web/kensei/\\_1363/soukoukeikaku2011/2011\\_Catalogue\\_eg/4\\_3\\_eg.html](http://www.pref.saga.lg.jp/web/kensei/_1363/soukoukeikaku2011/2011_Catalogue_eg/4_3_eg.html)

<sup>1</sup> [http://en.wikipedia.org/wiki/Disabled\\_parking\\_permit](http://en.wikipedia.org/wiki/Disabled_parking_permit)

<sup>2</sup> <https://www.gov.uk/apply-blue-badge>

<sup>3</sup> <http://www.nidirect.gov.uk/roads-service>

<sup>4</sup> [http://en.wikipedia.org/wiki/Americans\\_with\\_Disabilities\\_Act\\_of\\_1990](http://en.wikipedia.org/wiki/Americans_with_Disabilities_Act_of_1990)

provides another parking space for pregnant, elder persons and the others who need wheel chair. 1651 of parking lots are prepared DPP spaces already in Saga prefecture which include hospitals, Group Homes, shopping malls, etc. already. The DPP system is expanding to the other prefectures and cities. Currently, 30 prefectures and three cities adopted DPP system.

One of the biggest problems on DPP system is avoidance of car parking without permission. Due to the fact that the DPP spaces are shared by the cars without parking permission, the cars with permission cannot park their cars at the DPP spaces [1]. The paper proposes a DPP system allows avoiding car parking without permission.

In the next section, the proposed DPP system which allows avoiding car parking without permission is described followed by some experimental results. Then conclusion is described together with some discussions.

## II. PROPOSED DPP SYSTEM

### A. System Configuration

Process flow of the proposed DPP system is shown in Figure 1. The proposed DPP system has to detect cars in the designated DPP spaces. Also it has to distinguish the cars between with and without permission. After the system detects the cars without permission at the DPP space, some cautions are provided to such cars. These are components of the proposed system.

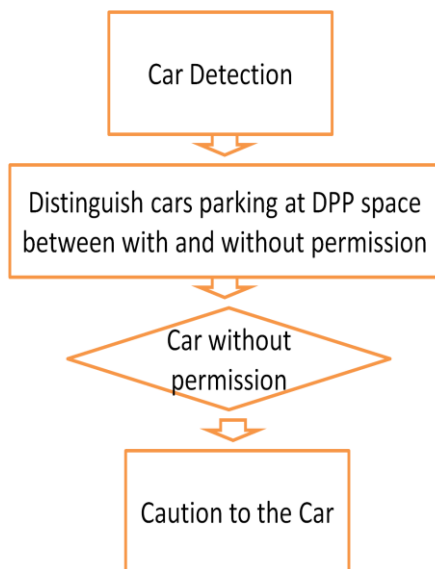


Fig. 1. Process flow of the proposed DPP system

Meanwhile, Figure 2 shows system configuration of the proposed DPP system. There are some alternatives for car detection system, caution system. Also, there are some candidates for caution system.

Hardware configuration includes, NIR LEDs, NIR camera, Ultrasonic sensor, RFID reader and writer, IC card, IC chip, GPS receiver, Mobile phone, ETC system, Tablet terminal or PC.

### B. Car Detection Systems

Cars have to be detected in day time and night time as well as in all weather conditions. Therefore, car monitoring cameras have to be visible and infrared cameras. Near Infrared: NIR cameras would be appropriate for car monitoring in day and night time and all weather conditions. NIR cameras require NIR light source. Otherwise, Signal to Noise ratio: SNR of NIR camera images would not be enough to recognize the plate number in concern. There are some commercially available NIR camera systems with NIR Light Emission Diodes: LEDs. It is not always that NIR camera system can detect cars in the designated DPP space due to heavy rain, or snow. Ultrasound sensor would work for car detection in such cases.



Fig. 2. System configuration of the proposed DPP system

On the other hand, there is another alternative. Using Radio Frequency Identification: RFID reader and writer, it is possible to identify DPPID holders. DPPID, in this case, is written in the specific IC card for DPPID, or other existing cards with IC chip for DPPID.

Another possibility of car detection is to use Electronic Toll Collection System: ETC system<sup>8</sup> for toll fee payment system. If the car equipped ETC system, then ETC signal can be read by the ETC receiving system.

GPS receiver is another possibility. Now a day, GPS receiver is available for almost cars. Even for the car without GPS receiver, it is possible to acquire their location data through GPS system containing in the mobile phones. Now a day, GPS receiver is equipped in the mobile phone in standard basis. If the car drivers with DPP registered to the ministry of transportation, then their location data can be available to acquire. Therefore, it is possible to find the car drivers are situated at the DPP space because the car drivers' mobile phones tell their location with a few meters of location estimation accuracy.

<sup>8</sup> ETC uses 5.8GHz center frequency of ISM band which is common frequency band for armature wireless communications. Data rate is 1024kbps based on Dedicated Short Range Communication: DSRC with ASK.

### C. Distinguish Cars Which Park DPP Space Between With and Without Permission

After the car detection, cars with and without DPP have to be distinguished each other. For the case of NIR camera monitoring system for car detection, plate number has to be recognized and then compare to the previously registered plate numbers in the DPP car plate numbers.

For the case with RFID reader and writer, it is possible to identify car drivers with DPP recorded on IC card or IC chip easily. On the other hand, it is possible to identify the cars with ETC identification code if the cars are registered as DPP holder with ETC identification code. Meanwhile, previously registered car drivers for their location identification with GPS receiver can be distinguished as DPP holder.

### D. Caution to the Car Without DPP

Next thing we have to do is make a caution to the car in the DPP space without DPP. There are three possible methods for making caution.

- 1) Caution with sound
- 2) Caution with flash light
- 3) Upload the photos of cars parking at DPP space without permission to YouTube

If car which is parking in DPP space without permission is found, a caution has to be announced to the car drivers with sound, "Do not park your car here because you do not have Disabled Parking Permit" or some other words. It is much more polite way to make caution with flash light. The third method is to avoid car parking without permission by uploading photos their cars with recognized plate number on YouTube. They are shamed when they look at the photos.

### E. Hardware Configuration

NIR camera with NIR LED of NET COWBOY DC-NCR131 camera is used. Major specification is as follows,

Interface: USB 1.1  
OS: Windows2000/XP  
Cable length: 1.5m  
Resolution (Pixel Size): 11280×1024  
Dimension: 52(W)×65(D)×70(H)mm  
Weight: 105g

There are 7 NIR LEDs just beside the camera mount of optical entrance.

ACER computer ASPIRE 5572 Series Core Duo T2050 1.6 GHz CPU and 1G of RAM is used for image processing, sound output, flashing light, ultrasonic sensor control, and camera control.

Principle of ultrasonic sensor is shown in Figure 3.

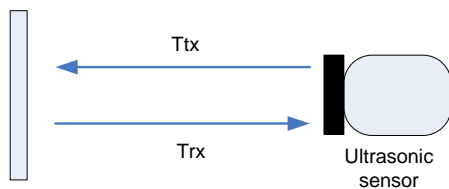


Fig. 3. Ultrasonic sensor, distance is measured by converting half of Ttx transmitting time and Trx receiving time

Ultrasonic sensor of T40-16 is used for car detection. Major specification of the sensor is as follows,

Frequency (kHz) 40  
Sound pressure level (dB) 115 <  
Sensitivity (dB) -64 <  
Dimension: Diameter 16.2, Height 12.2, Interval 10.0  
Measurable distance: 0.4-4m  
Unit of the measured distance: cm

Meanwhile, the MOD-RFID125 is used for reading IC card and/or IC chip for DPPID This RFID reader is USB type of RFID station, able to read Manchester-encoded 64-bit

EM4102 tags with 64 periods of carrier frequency per data bit. All the complexity of RFID tag detection, verification and decoding are handled by MOD-RFID125. After it strips the header and the checksums user is given the 40-bit ID of the transponder tag. Major specification of the RFID reader is as follows,

Supports Manchester-encoded 64-bit EM4102 RFID tags with 64 periods of carrier frequency per data bit;  
Base RFID frequency 125 kHz;  
USB port connection to PC;  
Standard 5V UART 9600, 8N1 connection to user microcontroller boards;  
Three modes of operation, easily changed by pressing the button;

- USB HID keyboard emulation mode;
  - USB CDC serial port emulation mode;
  - UART connection mode;
- Simple command-line interface in USB CDC and UART modes for configuration and data acquisition;  
Two LEDs indicating device status and tag presence;  
Support for continuous and periodic RF scanning to better suit user power requirements;  
Ships with default mode USB HID and default configuration: continuous read, scan always, one report per second, LEDs activated;

## III. EXPERIMENTS

### A. Ultrasonic Sensor

Experiments are conducted for assessment of distance measurement accuracy of the ultrasonic sensor used. Some objects are put in front of the sensor with varies distances, 0-3m. Ultrasonic sensor use PING type parallax product and microcontroller AT89S51 as processing data (convert from time value to distance output). Graph of accuracy sensor is shown in Figure 4.

Elevation angle is an important parameter for distance measuring accuracy of the sensor. This implies that the accuracy depends on sensor beam angle or width. Narrow beam allows a good accuracy because it is not affected due to influence with any disturbance. This experiment is conducted by measure elevation angle from 0 cm until 3 m. Figure 5 shows the relation between distance and elevation angle. Also, Figure 6 shows experimental results of the relation between elevation angle and distance measuring accuracy. Above portion of the graph shows the relation of distance versus

angle while below portion of graph shows the relation between the distances versus distance elevation.

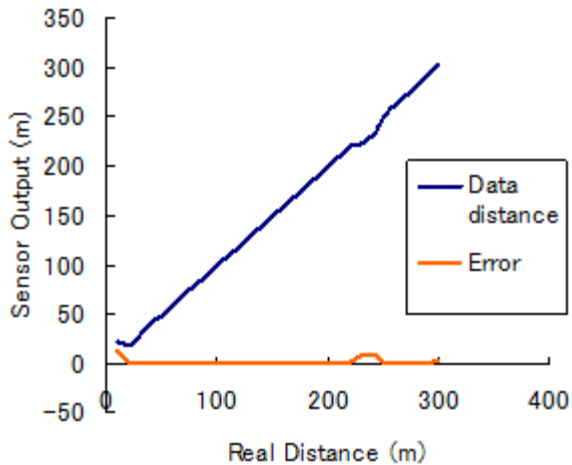


Fig.4. Experiment of ultrasonic accuracy. This shown that minimum distance is around 3 cm and maximum distance is 3 m. This range is appropriate for detect the object.

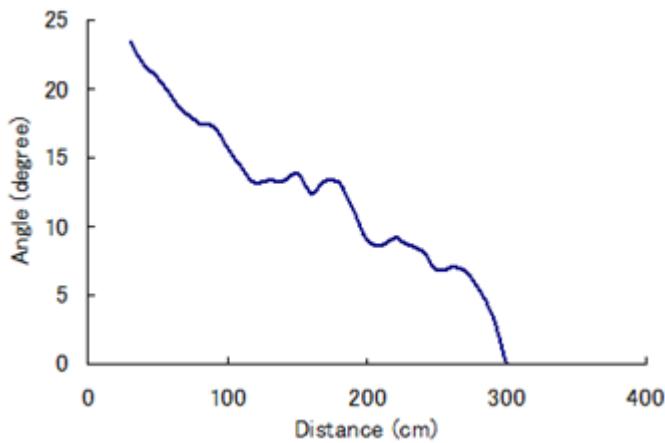


Fig. 5. Relation between distance and elevation angle.

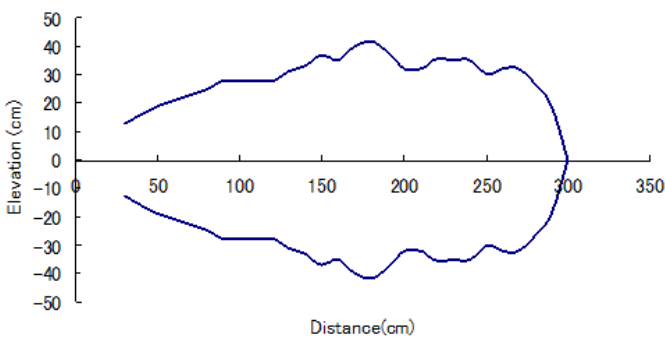


Fig. 6. Experiment of Elevation angle. Top side is distance versus angle, and bottom side is distance versus distance elevation.

Data is stored into computer by using USB communication. Results show that averaged processing time is 568.658 ms. Figure 7 also shows processing time of ultrasonic sensor. It looks that it takes longer time than the others.

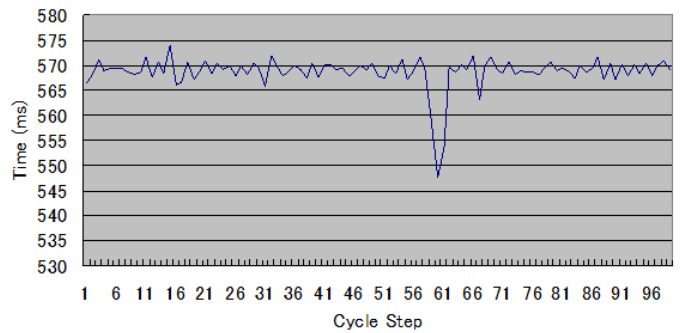


Fig. 7. Processing time of ultrasonic sensor.

### B. Number Plate Recognition

Figure 8 shows an example of the acquired image of the car which is parking at the parking lot. The example image is acquired in day time. The car in concern is situated in shaded area. Then the image is binarized with appropriate threshold. Figure 9 (a) shows the enhanced image while Figure 9 (b) shows binarized image with the determined threshold with histogram which is shown in Figure 9 (c).



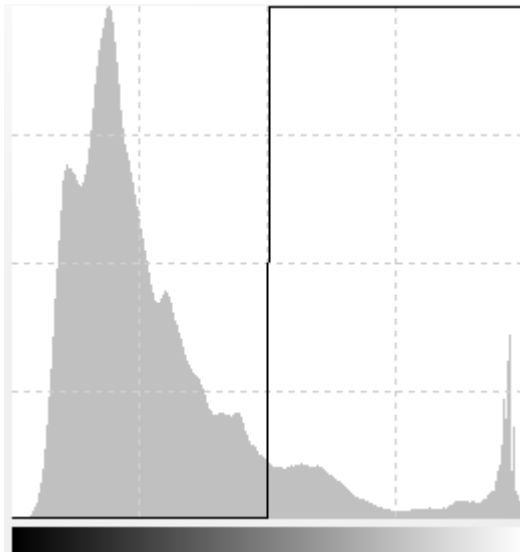
Fig. 8. Example of the acquired image of the car which is parking at the parking lot



(a)Enhanced image



(b)Binarized image



(c)Histogram of the original image



(d)Extracted image of the number plate in concern

Fig. 9. Processed images of day time acquisition before Optical Character Recognition: OCR

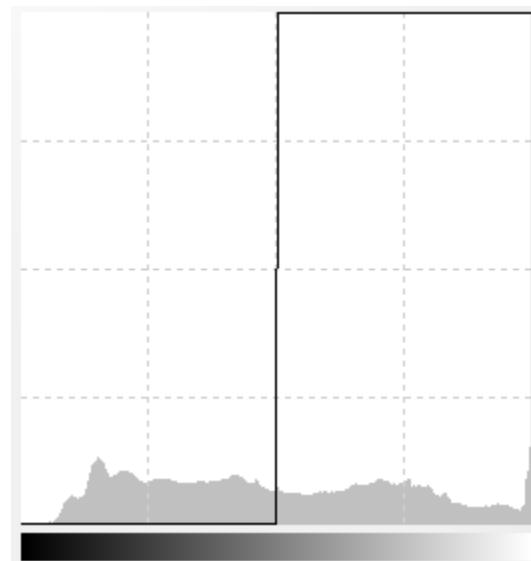
Then the number plate is extracted through blob likeness operator which is shown in Figure 9 (d)

These are same things for the acquired images in night time. The acquired image in night time is binarized with appropriate threshold. Figure 10 (a) shows the binarized image with the determined threshold with histogram which is shown

in Figure 10 (b). Also, Figure 10 (c) shows the extracted number plate for OCR.



(a)Binarized image



(b)Histogram of the original image



(c)Extracted image of the number plate in concern

Fig. 10. Processed images of night time acquisition before Optical Character Recognition: OCR

The images which are acquired in night time are dark and less contrast comparing to those which are acquired day time. The binarized images, however, are still recognizable for OCR. Using “nhocr” of OCR engine for Japanese language<sup>9</sup>, four

<sup>9</sup> <http://maggie.ocrgid.org/nhocr/>

digits of numerical characters are almost perfectly recognized. Comparison of the current plate number to the previously registered plate number is made for the four digits of numerical characters. Therefore, the first Kanji characters and small numerical numbers and small Hiragana character can be omitted.

### C. Location Estimations of the Registered Cars

The registered cars are available to estimate their location by using GPS system which is equipped their mobile phones. Figure 11 shows one example of the location of the registered car on a map.



Fig. 11. Example of the location of the registered car on a map.

The locations of the registered cars are updated every one second with a couple of m of location estimation accuracy. The time interval of 1 second is good enough. Yellow dots show the location with every one second time interval. Meanwhile, a couple of m of location estimation accuracy would be marginal. The estimated location is compared to the location of DPP space. If these are matched, then the car in the DPP space is permitted. If cars are detected in the specific DPP space by ultrasonic sensor, and if there is no indication of registered car in the DPP space, caution is made to the car.

## IV. CONCLUSION

Cheap and effective system for parking avoidance of the car without permission at Disabled Parking Permit: DPP space is proposed. The proposed system is validated through some experiments. Multiple methods for detection of car in the DPP space using ultrasound sensors, Near Infrared: NIR cameras, RFID writer and reader with IC card, IC chip and IC tag as well as ETC system and GPS receiver are proposed. It is found that these proposed car detection systems work well. Furthermore, it is effective if more than two systems out of the proposed car detection systems are used for avoid car parking without permission.

It is found that considerable combination of more than two methods proposed here would be useful and effective to avoid the car parking without DPP permission.

## ACKNOWLEDGMENT

The author would like to thank Professor Dr. Masaru Kiyota of Saga University for his valuable discussions we have had through research works. Also, the author would like to thank Dr. Steven Ray Sentinuwo for his efforts to conduct experiments and simulations.

## REFERENCES

- [1] Arai, K, Introducing IT technologies to Disabled Parking Permit, Saga University Organized Sympojium on Diabled Parking Permit, 2013.

## AUTHORS PROFILE

**Kohei Arai**, He received BS, MS and PhD degrees in 1972, 1974 and 1982, respectively. He was with The Institute for Industrial Science and Technology of the University of Tokyo from April 1974 to December 1978 also was with National Space Development Agency of Japan from January, 1979 to March, 1990. During from 1985 to 1987, he was with Canada Centre for Remote Sensing as a Post Doctoral Fellow of National Science and Engineering Research Council of Canada. He moved to Saga University as a Professor in Department of Information Science on April 1990. He was a councilor for the Aeronautics and Space related to the Technology Committee of the Ministry of Science and Technology during from 1998 to 2000. He was a councilor of Saga University for 2002 and 2003. He also was an executive councilor for the Remote Sensing Society of Japan for 2003 to 2005. He is an Adjunct Professor of University of Arizona, USA since 1998. He also is Vice Chairman of the Commission "A" of ICSU/COSPAR since 2008. He wrote 30 books and published 442 journal papers

# Noise Suppressing Edge Enhancement Based on Genetic Algorithm Taking Into Account Complexity of Target Images Measured with Fractal Dimension

Kohei Arai<sup>1</sup>

Graduate School of Science and Engineering  
Saga University  
Saga City, Japan

**Abstract**—Method for noise suppressing edge enhancement based on genetic algorithm taking into account complexity of target images measured with fractal dimension is proposed. Through experiments with satellite remote sensing imagery data with additive noise, it is found that the proposed method shows appropriate edge enhancing performance with suppressing the additive noise in accordance with complexity of target images. It is also found that the proposed method requires a small computer resources in comparison to the method based on Simulated Annealing: SA.

**Keywords**—edge enhancement; fractal dimension; genetic algorithm; simulated annealing; remote sensing satellite imagery

## I. INTRODUCTION

There are many edge enhancement methods in the field of image processing and analysis. Differentiation of images is just one example of the methods<sup>1</sup>. Prewitz operator, Sobel operator<sup>2</sup>, Laplace operator<sup>3</sup>, Un-Sharp masking<sup>4</sup>, Canny filter<sup>5</sup> etc. are typical edge enhancement operators. On the other hand, there are also many methods of smoothing filter<sup>6</sup> for noise suppressions. Averaging filter<sup>7</sup>, Median filter<sup>8</sup>, Gaussian filter<sup>9</sup>, etc. are typical smoothing filter. Most of cases of image processing and analysis requires edge enhancement with noise suppressions. Therefore, these edge enhancements and smoothing filters are applied to target images simultaneously or sequentially [1].

The most appropriate edge enhance method depends on characteristics of the target images, in particular, complexity of the target images. For instance, simple images do not have many edges while there are many edges in complex images. Therefore, it would better to take into account image complexity in parameter estimations of edge enhancement methods. Fractal dimension is one of the complexity representation methods. Hausdorff dimension<sup>10</sup>, Rényi

dimension<sup>11</sup>, Packing dimension<sup>12</sup> are typical theoretical fractal dimensions. However, Minkowski–Bouligand dimension<sup>13</sup>, Correlation dimension<sup>14</sup> are widely used to use because these are relatively easy to calculate [2]. Therefore, probabilistic auto-correlative dimension is for representation of complexity of the target images in the paper.

Finding the most appropriate edge enhancement method is a kind of optimization problem solving. Namely, edge enhancement method with the most appropriate parameter set is obtained by using optimization problem solving in accordance with input image characteristics. There are some methods for optimization problem solving, linear and non-linear optimization to find global optimum or local minima. Only the Simulated Annealing: SA ensure finding global optimum solution while some other optimization methods, such as Steepest Descent Method: SDM, Conjugate Gradient Method: CGM (Newton Raphson method), Genetic Algorithm: GA, etc. find one of local minima solutions. SA requires huge computer resources while the other methods require not so large computer resources [3].

The edge enhancement method with suppressing noise is based on LOG filter which apply Gaussian filter first and then apply Un-Sharp Masking followed by, taking into account input image characteristics of complexity which is detected by probabilistic auto-correlative dimension. Based on GA with appropriate parameters of cross-over, mutation, fitness function is defined with the complexity and the ratio of power spectrum of input and output images. In prior to apply the proposed edge enhancement method, median filter is applied for elimination of isolated noise pixels.

Experiments with remote sensing satellite images are conducted to validate the proposed edge enhancement method. The results show that output edge enhanced images with the proposed method and that from the SA based method are almost similar. Meanwhile, computation resources required for the proposed GA based method is almost 1/53 comparing to

<sup>1</sup> <http://www.mis.med.akita-u.ac.jp/~kata/image/sobelprew.html>

<sup>2</sup> [http://en.wikipedia.org/wiki/Sobel\\_operator](http://en.wikipedia.org/wiki/Sobel_operator)

<sup>3</sup> [http://en.wikipedia.org/wiki/Discrete\\_Laplace\\_operator](http://en.wikipedia.org/wiki/Discrete_Laplace_operator)

<sup>4</sup> [http://en.wikipedia.org/wiki/Unsharp\\_masking](http://en.wikipedia.org/wiki/Unsharp_masking)

<sup>5</sup> [http://en.wikipedia.org/wiki/Canny\\_edge\\_detector](http://en.wikipedia.org/wiki/Canny_edge_detector)

<sup>6</sup> <http://en.wikipedia.org/wiki/Smoothing>

<sup>7</sup> <http://homepages.inf.ed.ac.uk/rbf/HIPR2/mean.htm>

<sup>8</sup> [http://en.wikipedia.org/wiki/Median\\_filter](http://en.wikipedia.org/wiki/Median_filter)

<sup>9</sup> [http://en.wikipedia.org/wiki/Gaussian\\_filter](http://en.wikipedia.org/wiki/Gaussian_filter)

<sup>10</sup> [http://en.wikipedia.org/wiki/Hausdorff\\_dimension](http://en.wikipedia.org/wiki/Hausdorff_dimension)

<sup>11</sup>

<http://ja.wikipedia.org/wiki/%E3%83%95%E3%83%A9%E3%82%AF%E3%82%BF%E3%83%AB%E6%AC%A1%E5%85%83#.E3.83.AC.E3.83.8B.E3.83.BC.E6.AC.A1.E5.85.83>

<sup>12</sup> [http://en.wikipedia.org/wiki/Packing\\_dimension](http://en.wikipedia.org/wiki/Packing_dimension)

<sup>13</sup> [http://en.wikipedia.org/wiki/Box-counting\\_dimension](http://en.wikipedia.org/wiki/Box-counting_dimension)

<sup>14</sup> [http://en.wikipedia.org/wiki/Correlation\\_dimension](http://en.wikipedia.org/wiki/Correlation_dimension)

that for the SA based method. Therefore, the proposed method is efficiently and effectively useful in comparison to the SA based method.

The following section describes the proposed method followed by some experimental results. Then finally concluding remarks is described together with some discussions.

## II. PROPOSED METHOD

### A. LOG Filter

The proposed edge enhancement method is based on LOG filter which is defined as follows,

Firstly, Gaussian filter is applied to input images followed by Un-Sharp Masking. Gaussian filter is defined in equation (1).

$$g(j, i) = \sum_{y=-n}^n \sum_{x=-n}^n gauss(x, y) f(j+x, i+y) \quad (1)$$

where  $f(j, i)$  and  $g(j, i)$  denotes input and output images, two dimensional gray level in direction of line, pixel coordinates,  $j$  and  $i$  ( $x$  and  $y$ ). Meanwhile,  $n$  denotes image pixel size in directions of line and pixel. On the other hand,  $gauss(x, y)$  is expressed in equation (2).

$$gauss(x, y) = \frac{\exp(-\frac{x^2+y^2}{2\sigma^2})}{2\pi\sigma^2} \quad (2)$$

Also, Un-Sharp masking is defined as equation (3).

$$g(j, i) = f(j, i) - \nabla^2 f(j, i) \quad (3)$$

where  $\nabla^2$  denotes Laplace operator which is second order of differentiation of equation (4).

$$\nabla^2 f(x, y) = \frac{\partial^2 f(x, y)}{\partial x^2} \mathbf{j} + \frac{\partial^2 f(x, y)}{\partial y^2} \mathbf{i} \quad (4)$$

Thus, LOG filter is defined as equation (5).

$$h(j, i) = g(j, i) - \nabla^2 g(j, i) \quad (5)$$

### B. Genetic Algorithm Based Edge Enhancement

Fitness function which represents edge information is very important for GA based edge enhancements. Edge enhancement implies high frequency component enhancement. Therefore, the ratio of frequency components of input and output images would be used for a fitness function as defined in equation (6).

$$F_I = \frac{P_{I_{original}}}{P_{I_{transformed}}} \quad (6)$$

where  $P^*$  denotes power spectrum while  $I_{original}$  and  $I_{transformed}$  denotes input and output images.

In the mean time, noise has to be suppressed as much as we can. Low pass filter is used for noise suppression. In general, noise spectrum is widely spreaded from zero to infinitive frequency components. Signal frequency component is degraded when the cut-off frequency of low pass filter is too low, noise can be suppressed greatly though. Therefore, a filter which allows to suppress higher frequency component maintaining edge components which are also higher frequency components is considered. The frequency has to be normalized because Nyquist frequency of images depends on image size. Therefore, normalized frequency is defined in equation (7).

$$f = \frac{\sqrt{f_x^2 + f_y^2}}{f_N} \quad (7)$$

where  $f_N$  denotes Nyquist frequency while  $f_x$  and  $f_y$  denotes frequency in direction of line and pixel. Furthermore, it would be better to normalize the frequency as follows,

when frequency is zero while Nyquist frequency is  $f_N$ , the normalized frequency is one. Therefore, the following weighting function is applied to frequency,

$$w(f) = a \cdot \exp(f^{10}) + b \quad (8)$$

where  $w(0) = 0, w(1) = 1$  then

$$\begin{cases} 0.0 = a \cdot \exp(0.0^{10}) + b \\ 1.0 = a \cdot \exp(1.0^{10}) + b \end{cases} \quad (9)$$

Therefore,  $a$  and  $b$  can be determined in equation (10).

$$\begin{cases} a = 1/(e-1) \\ b = -1/(e-1) \end{cases} \quad (10)$$

Thus the equation (8) can be rewritten by equation (11).

$$w(f) = \frac{\exp(f^{10}) - 1}{e - 1} \quad (11)$$

As is mentioned before, fitness function is also normalized within the range of  $[0, \sqrt{2}]$ . Power spectrum  $p(f_I)$  of the image  $I$  is defined and also weighted sum of  $p(f_I)$  can be defined in equation (12)

$$P_I = \sum_{f_I=0}^{f_N} w(f_I) \cdot p(f_I) \quad (12)$$

Thus fitness function of equation (6) is derived with the normalized and weighted sum of power spectrum,  $P^*$  ( $*$  denotes input  $I_{original}$  and output images  $I_{transformed}$ ).

### C. Image Complexity

Probabilistic auto-correlative dimension is used for representation of complexity of the target images. Let  $F(at)$  be a stochastic process as  $\forall a > 0$ .

$$F(at) = a^H F(t) \quad (13)$$

where  $F(t)$  is a self-similar type of stochastic process with the power of  $H$ . The equation (13) implies that the probability density function of  $F(at)$  is identical to that of  $a^H F(t)$ . Thus probabilistic self-similar dimension  $H$  can be written in equation (14) through taking logarithmic function of expectation (E) maintaining  $t$ .

$$H = \frac{-\log_{10}\left(\frac{E[F(at)]}{E[F(t)]}\right)}{\log_{10}\left(\frac{1}{a}\right)} \quad (14)$$

With the fixing  $t=1$ ,  $N\left(\frac{1}{a}\right)$  of surface division number of image grey-level of curved surface is defined as of image is divided into  $\frac{1}{a} \times \frac{1}{a}$ . In other word, the number of division of  $E[F(a)]$  with the unit length of  $1/a$  is defined as  $N\left(\frac{1}{a}\right)$ . Taking logarithmic function of  $N\left(\frac{1}{a}\right)$ , equation (14) can be rewritten by equation (15).

$$\log_{10} N(r) = -H \log_{10} r + \log_{10} N(1) \quad (15)$$

where  $r$  denotes  $1/a$ . In general,  $H$  is varied depending on  $r$ . Edge components are maintained if the target image can be represented as fractal like images. Therefore, fractal dimension  $H$  can be determined through regressive analysis based on least square method with sample values of

$$(\log_{10} r, \log_{10} N(r)), (r = 1, 2, \dots)$$

If the surface area of  $S(r)$  can be written in equation (16),

$$S(r) = r^2 \cdot N(r) \quad (16)$$

where the target image is divided into  $r \times r$ , then the equation (16) can be rewritten by equation (17)

$$\log_{10} S(r) = (2 - H) \log_{10} r + \log_{10} S(1) \quad (17)$$

Thus fractal dimension can be calculated as estimation value of  $2 - H$  through regression analysis with

$$(\log_{10} r, \log_{10} S(r)), (r = 1, 2, \dots)$$

based on least square method.

### D. Fitness Function of GA for Edge Enhancement

Fractal dimension of grey-level images (half tone images)  $D_I$  is within the range of 2 to 3,  $2 \leq D_I < 3$ . In order to

normalize  $D_I$  within the range of [0,1],  $D_I - 2$  is adopted as fitness function. Taking into account the aforementioned normalized frequency components ratio,  $F_i$ , the fitness function  $f_i$  is defined as follows,

$$f_i = (D_I - 2)F_i \quad (18)$$

Thus the edge enhancement method with suppressing noise is based on LOG filter which apply Gaussian filter first and then apply Un-Sharp Masking followed by, taking into account input image characteristics of complexity which is detected by probabilistic auto-correlative dimension is defined. Based on GA with appropriate parameters of cross-over, mutation, fitness function is defined with the complexity and the ratio of power spectrum of input and output images. In prior to apply the proposed edge enhancement method, median filter is applied for elimination of isolated noise pixels.

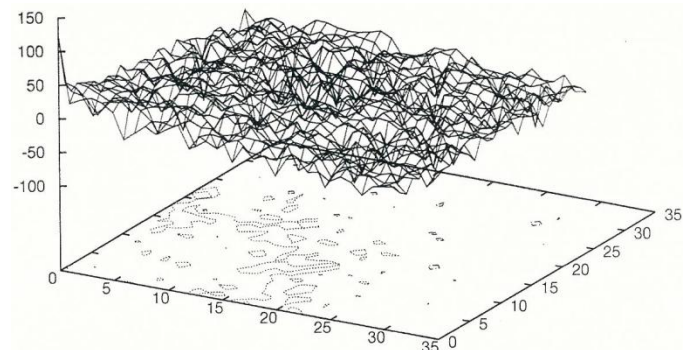
## III. EXPERIMENTS

### A. Data Used

32 by 32 pixels of a portion of Landsat TM imagery data [4] of Saga city in Kyushu, Japan is used for the experiments. Original image is shown in Fig.1 together with frequency component in direction of line and pixel.



(a)Original image of 32 by 32 pixels of a portion of Landsat TM imagery data of Saga city in Kyushu, Japan



(b) Frequency component of the original image in direction of line and pixel

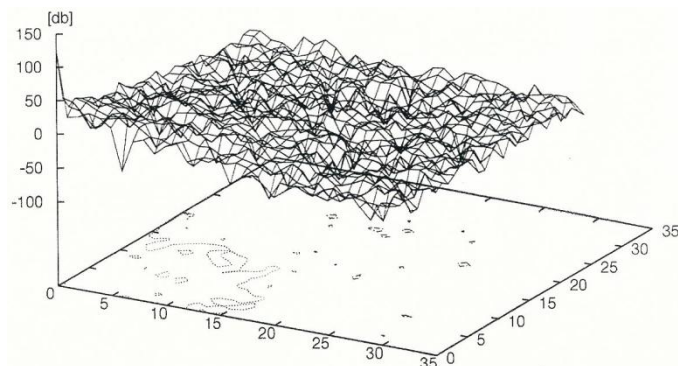
Fig. 1. Original image of 32 by 32 pixels of a portion of Landsat TM imagery data of Saga city in Kyushu, Japan and its 2D spectrum distribution.

### B. Effect of Median Filter

In order to eliminate isolated noise pixels which are contained in the original image, median filter is applied to the original image. The resultant image is shown in Fig.2 together with its frequency component in direction of line and pixel. 2D spectrum of Fig.2 (b) shows how the isolated noise pixels are eliminated maintaining major frequency components.



(a) Resultant image after applying median filter to the original image of 32 by 32 pixels of a portion of Landsat TM imagery data of Saga city in Kyushu, Japan



(b) Frequency component of the resultant image in direction of line and pixel

Fig. 2. Resultant image after applying median filter to the original image of 32 by 32 pixels of a portion of Landsat TM imagery data of Saga city in Kyushu, Japan and its 2D spectrum distribution.

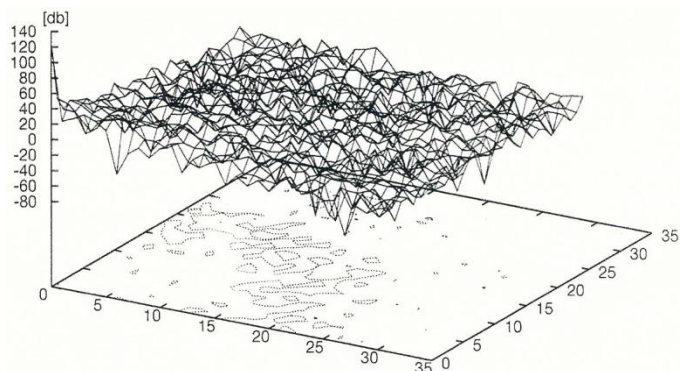
### C. Effect of Additive Noise

By using Mersenne Twister of random number generator [5], 30% of averaged frequency component of the original image of Gaussian noise is added to the original image. Fig.3 shows the noise added image together with frequency component in direction of line and pixel.

Also, Fig.4 shows the resultant image after applying median filter to the 30% of noise added original image of 32 by 32 pixels of a portion of Landsat TM imagery data of Saga city in Kyushu, Japan and its 2D spectrum distribution.



(a) 30% of noise added original image of 32 by 32 pixels of a portion of Landsat TM imagery data of Saga city in Kyushu, Japan

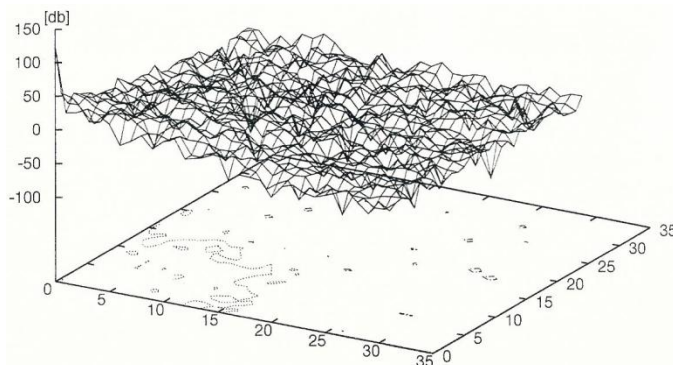


(b) Frequency component of the noise added image in direction of line and pixel

Fig. 3. 30% of noise added original image of 32 by 32 pixels of a portion of Landsat TM imagery data of Saga city in Kyushu, Japan and its 2D spectrum distribution.



(a) Resultant image after apply median filter to the 30% of noise added original image of 32 by 32 pixels of a portion of Landsat TM imagery data of Saga city in Kyushu, Japan



(b) Frequency component of the resultant image in direction of line and pixel

Fig. 4. Resultant image after applying median filter to the 30% of noise added original image of 32 by 32 pixels of a portion of Landsat TM imagery data of Saga city in Kyushu, Japan and its 2D spectrum distribution.

Meanwhile, Fig.5 shows 50% of noise added original image of 32 by 32 pixels of a portion of Landsat TM imagery data of Saga city in Kyushu, Japan and its 2D spectrum distribution.

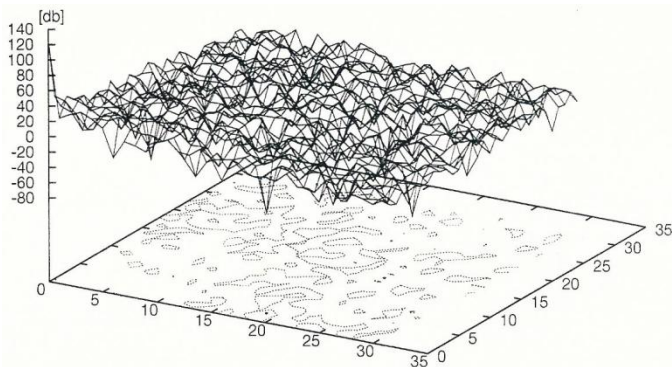
On the other hand, Fig.6 shows the resultant image after applying median filter to the 50% of noise added original image of 32 by 32 pixels of a portion of Landsat TM imagery data of Saga city in Kyushu, Japan and its 2D spectrum distribution. From these Fig.4 and 6, it is found that median filter does work for isolated noise pixels. Also, higher frequency component increases in accordance with increasing added noise obviously.

**D. Effect of the Proposed Edge Enhancement Method**

Using same imagery data, the proposed LOG filter based edge enhancement method based on GA is evaluated. In the experiments, cross-over probability is set at 0.21 and mutation probability is set at 0.05. These parameters for GA are found empirically.



(a) 50% of noise added original image of 32 by 32 pixels of a portion of Landsat TM imagery data of Saga city in Kyushu, Japan

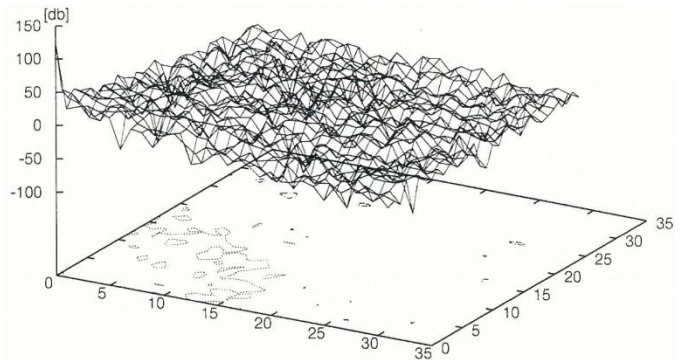


(b) Frequency component of the noise added image in direction of line and pixel

Fig. 5. 50% of noise added original image of 32 by 32 pixels of a portion of Landsat TM imagery data of Saga city in Kyushu, Japan and its 2D spectrum distribution.



(a) Resultant image after applying median filter to the 50% of noise added original image of 32 by 32 pixels of a portion of Landsat TM imagery data of Saga city in Kyushu, Japan



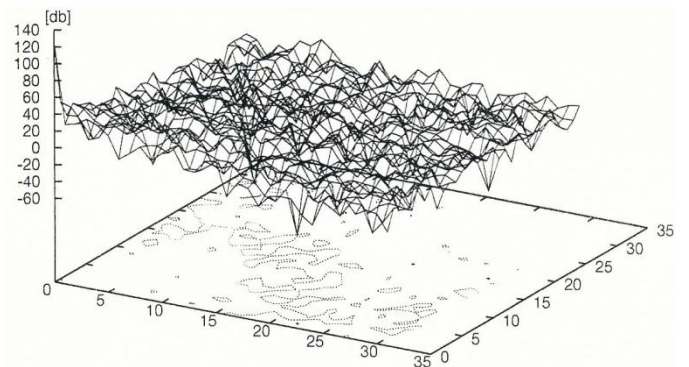
(b) Frequency component of the resultant image in direction of line and pixel

Fig. 6. Resultant image after applying median filter to the 50% of noise added original image of 32 by 32 pixels of a portion of Landsat TM imagery data of Saga city in Kyushu, Japan and its 2D spectrum distribution.

Fig.7 and 8 shows the resultant images after applying the proposed method to 30% and 50% of noise added original image and their 2D spectra, respectively. Through comparison between Fig.7, Fig.8 and Fig.3, Fig.5, respectively, it is found that the proposed edge enhancement method does work for enhancing edges depending on the complexity of the image in concern with noise suppression.



(a) Resultant image after applying the proposed edge enhancement method based on GA to the 30% of noise added original image of 32 by 32 pixels of a portion of Landsat TM imagery data of Saga city in Kyushu, Japan

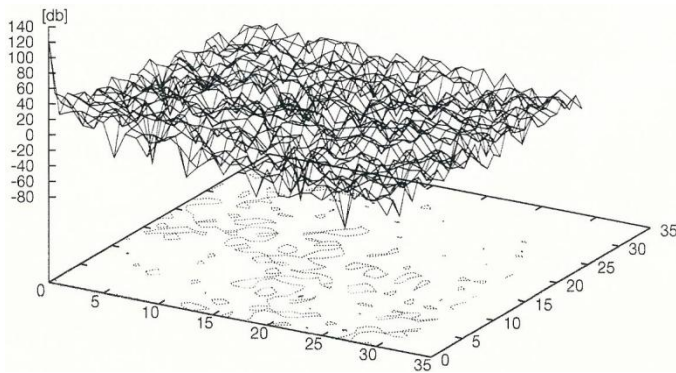


(b) Frequency component of the resultant image in direction of line and pixel

Fig. 7. Resultant image after applying the proposed edge enhancement method based on GA to the 30% of noise added original image of 32 by 32 pixels of a portion of Landsat TM imagery data of Saga city in Kyushu, Japan and its 2D spectrum distribution.



(a) Resultant image after applying the proposed edge enhancement method based on GA to the 50% of noise added original image of 32 by 32 pixels of a portion of Landsat TM imagery data of Saga city in Kyushu, Japan



(b) Frequency component of the resultant image in direction of line and pixel

Fig. 8. Resultant image after applying the proposed edge enhancement method based on GA to the 50% of noise added original image of 32 by 32 pixels of a portion of Landsat TM imagery data of Saga city in Kyushu, Japan and its 2D spectrum distribution.

#### E. Comparison to the Edge Enhancement Method Based on SA

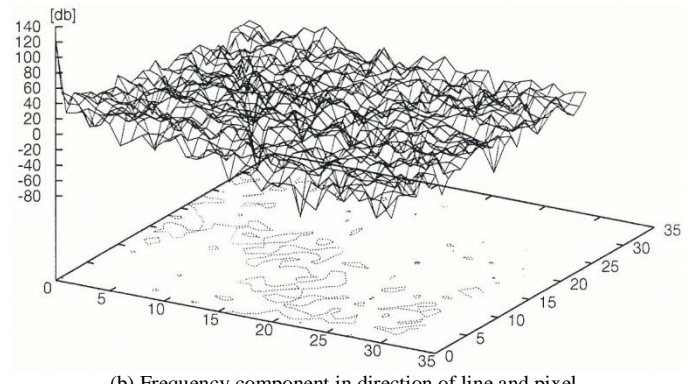
Using same imagery data, the proposed LOG filter based edge enhancement method based on GA is compared to the edge enhancement method based on SA. Fig.9 and 10 shows the resultant images after applying the SA based method to 30% and 50% of noise added original image and their 2D spectra, respectively. Through comparison between Fig.9, Fig.10 and Fig.7, Fig.8, respectively, it is found that the resultant images of the proposed edge enhancement method are almost same as the resultant images derived from the SA based edge enhancement method.

Both GA based and SA based edge enhancement methods work well for enhancing edges depending on the complexity of the image in concern with noise suppression. The number of iteration of GA is 164670 while that of SA is 8783578. These numbers are found empirically with the convergence condition of residual error of 5%. Namely, the proposed edge enhancement method is 53.34 times faster than the SA based method with almost same edge enhancement performance.

In comparison between the proposed edge enhancement method and median filter method, the resultant images after applying median filter show that it does not work for edge enhancement while noise suppression performance is good though. On the other hand, the proposed GA based edge enhancement method does work for edge enhancement with noise suppressing performance.

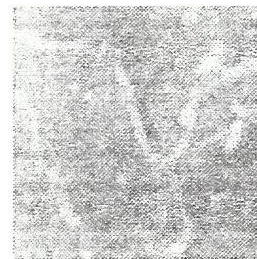


(a) Resultant image after applying the proposed edge enhancement method based on SA to the 30% of noise added original image of 32 by 32 pixels of a portion of Landsat TM imagery data of Saga city in Kyushu, Japan

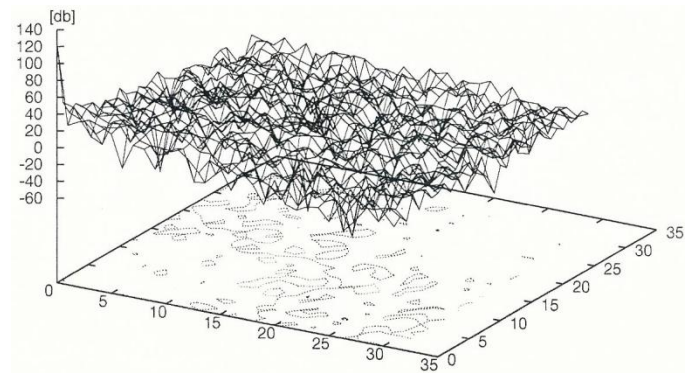


(b) Frequency component in direction of line and pixel

Fig. 9. Resultant image after applying the proposed edge enhancement method based on SA to the 30% of noise added original image of 32 by 32 pixels of a portion of Landsat TM imagery data of Saga city in Kyushu, Japan and its 2D spectrum distribution.



(a) Resultant image after applying the proposed edge enhancement method based on SA to the 50% of noise added original image of 32 by 32 pixels of a portion of Landsat TM imagery data of Saga city in Kyushu, Japan



(b) Frequency component in direction of line and pixel

Fig. 10. Resultant image after applying the proposed edge enhancement method based on SA to the 50% of noise added original image of 32 by 32 pixels of a portion of Landsat TM imagery data of Saga city in Kyushu, Japan and its 2D spectrum distribution.

#### IV. CONCLUSION

LOG filter based method for noise suppressing edge enhancement based on Genetic Algorithm: GA taking into account complexity of target images measured with fractal dimension is proposed. Through experiments with satellite remote sensing imagery data with additive noise, it is found that the proposed method shows appropriate edge enhancing performance with suppressing the additive noise in accordance with complexity of target images. It is also found that the proposed method requires a small computer resources in comparison to the method based on Simulated Annealing: SA.

Through experiments with Landsat TM imagery data of Saga city, Kyushu, Japan, it is found that the proposed GA based edge enhancement method does work for edge enhancement depending on complexity of image with a good noise suppressing performance. The number of iteration of GA is 164670 while that of SA is 8783578. These numbers are found empirically with the convergence condition of residual error of 5%. Namely, the proposed edge enhancement method is 53.34 times faster than the SA based method with almost same edge enhancement performance.

#### ACKNOWLEDGMENT

The author would like to thank Mr. Mitsuki Nakamura for his efforts through experiments and simulations.

#### REFERENCES

- [1] Arai, K., Lecture note for image processing, Gakujutsu-Tosho-Shuppan publishing Co. Ltd., 1999.
- [2] Arai, K., Remote Sensing Satellite image processing methods with Java programing language, Morikita Shuppan publishing Co. Ltd., 2001.
- [3] Arai, K., Fundamental theory for pattern recognition, Gakujutsu Tosho Shuppan, Publishing Co. Ltd., 1999.
- [4] Arai, K, Lecture Notes on Remote Sensing, Morikita-Shuppan, Co.Ltd., 2005
- [5] Mersenne Twister (MT), <http://www.math.sci.hiroshima-u.ac.jp/~m-mat/MT/mt.html>

#### AUTHORS PROFILE

**Kohei Arai**, He received BS, MS and PhD degrees in 1972, 1974 and 1982, respectively. He was with The Institute for Industrial Science and Technology of the University of Tokyo from April 1974 to December 1978 also was with National Space Development Agency of Japan from January, 1979 to March, 1990. During from 1985 to 1987, he was with Canada Centre for Remote Sensing as a Post Doctoral Fellow of National Science and Engineering Research Council of Canada. He moved to Saga University as a Professor in Department of Information Science on April 1990. He was a councilor for the Aeronautics and Space related to the Technology Committee of the Ministry of Science and Technology during from 1998 to 2000. He was a councilor of Saga University for 2002 and 2003. He also was an executive councilor for the Remote Sensing Society of Japan for 2003 to 2005. He is an Adjunct Professor of University of Arizona, USA since 1998. He also is Vice Chairman of the Commission "A" of ICSU/COSPAR since 2008. He wrote 30 books and published 322 journal papers

# Comparison Among Cross, Onboard and Vicarious Calibrations for Terra/ASTER/VNIR

Kohei Arai <sup>1</sup>

Graduate School of Science and Engineering  
Saga University  
Saga City, Japan

**Abstract**—Comparative study on radiometric calibration methods among onboard, cross and vicarious calibration for visible to near infrared radiometers onboard satellites is conducted. The data sources of the aforementioned three calibration methods are different and independent. Therefore, it may say that the reliable Radiometric Calibration Accuracy: RCC would be the RCC which are resemble each other two of three RCCs. As experimental results, it is found that vicarious and cross calibration are reliable than onboard calibration. Also vicarious calibration based cross calibration method is proposed here. The proposed cross calibration method should be superior to the conventional cross calibration method based on band-to-band data comparison. Through experiments, it is also found that the proposed cross calibration is better than the conventional cross calibration. The radiometric calibration accuracy of the conventional cross calibration method can be evaluated by using the proposed cross calibration method.

**Keywords**—vicarious calibration; cross calibration; visible to near infrared radiometer; earth observation satellite; remote sensing; radiative transfer equation

## I. INTRODUCTION

There are many previous research works on calibration of solar reflective wavelength coverage of mission instruments onboard remote sensing satellites [1]-[17]. It is obvious that onboard calibration sources are degraded for time being (Dinguirard and Slater (1999)). Not only radiometer, but also onboard calibration system is degraded together with calibration system monitoring systems. There are onboard, cross and vicarious calibrations. These calibrations use the different data sources. Therefore, Radiometric Calibration Coefficient: RCC for one of three calibration methods can be checked with the other calibration methods. Thus much reliable RCC would be obtained.

Usually, the conventional cross calibration can be done through comparisons of band-to-band data of which spectral response functions are overlapped mostly. There are the following major error sources due to observation time difference, spectral response function difference in conjunction of spectral surface reflectance and spectral atmospheric optical depth, observation area difference. These error sources are assessed with dataset acquired through ground measurements of spectral surface reflectance and spectral optical depth. Then the accuracy of the conventional cross calibration is evaluated with vicarious calibration data.

Several researchers investigated cross calibration. Teillet,

Fedosejevs, Thome, and Barker (2007) investigated impact of spectral response difference effect between sensors as quantitative indication using simulated data of observation [19]. The effect is called SBDE (Spectral Band Difference Effect) in this research. Twenty sensors were considered in the simulation together with some ground types, various combinations of atmospheric states and illumination geometries. They argued, overall, if spectral band difference effects (SBDEs) are not taken into account, the Railroad Valley Playa site is a 'good' ground target for cross calibration between most but not all satellite sensors in most but not all spectral regions investigated. 'Good' is denoted as SBDEs within 3%.

Liu, Li, Qiao, Liu, and Zhang (2004) developed a new method for cross calibration, and then applied the method to sensors Multi-channel Visible Infrared Scanning radiometers (MVIRS) and Moderate Resolution Imaging Spectroradiometer (MODIS) [18]. They argued, "Error analysis indicates that the calibration is accurate to within 5%, which is comparable to, or better than, the vicarious calibration method".

The method considers surface bidirectional reflectance distribution function (BRDF) mainly. BRDF indicates distribution of angle of reflection depend on an angle of incidence of illumination on the surface. In these researches, differences of SRF do not be considered. If the impact of its difference can be considered on cross calibration, differences between observed data can be explained more exactly and we can implement cross calibration by higher reliability.

ASTER/VNIR is onboard Terra satellite and is calibrated with onboard calibration sources [20], vicarious calibration data as well as cross calibration. MODIS is onboard same platform and is calibrated with the aforementioned several types of data [21]. This situation is same thing for MISR [22] and ETM+ onboard the different platform, Landsat-7 [23].

The method proposed here is to check a reliability of the calibration sources through vicarious and cross calibrations for validations of these calibration accuracies. Namely, vicarious calibration requires spectral surface reflectance measurements and spectral optical thickness measurements. By using these ground based acquired data, cross calibration is conducted to improve a reliability of the calibration sources through comparison of vicarious calibration data. The results show that cross calibration accuracy can be done much more precisely if the influences due to the aforementioned three major error

sources are taken into account.

## II. PROPOSED METHOD

### A. Cross Calibration

The mission instrument in concern is VNIR: Visible to Near Infrared Radiometer of ASTER: Advanced Spectrometer for Thermal Emission and Reflectance onboard Terra satellite. Other instruments of which wavelength coverage are overlapped are onboard the same Terra satellite. Namely, the wavelength coverage of MODIS and MISR are overlapped with ASTER/VNIR. The wavelength coverage of these mission instruments are shown in Table 1 together with IFOV: Instantaneous Field of View.

Other than these, the wavelength coverage of ETM+ onboard Landsat-5 is also overlapped with that of ASTER/VNIR. Therefore, cross calibration can be done between ASTER/VNIR and MODIS, MISR, ETM+. In MISR, these wavelengths are center wavelength of band. MISR bandwidth in Green, Red, and NIR are 0.028, 0.022, 0.039 micrometer, respectively.

TABLE I. MAJOR SPECIFICATION OF FOUR RADIOMETERS IN CONCERN FOR CROSS CALIBRATION BETWEEN ASTER/VNIR AND THE OTHER THREE RADIOMETERS

	ASTER (15m/px)	MISR (275m/px)	MODIS (250m/px)	ETM+ (30m/px)
Green	0.52 - 0.60 (band1)	0.558	none	0.52 - 0.60 (band2)
Red	0.63 - 0.69 (band2)	0.672	0.62 - 0.67 (band1)	0.63 - 0.69 (band3)
NIR	0.76 - 0.86 (band3N)	0.867	0.84 - 0.87 (band2)	0.75 - 0.90 (band4)

### B. Vicarious Calibration

Vicarious calibration coefficients, on the other hand, is defined as the difference between ASTER/VNIR pixel value derived radiance and the estimated radiance derived from the radiative transfer equation with the input parameters of surface reflectance measured on the ground, refractive index and size distribution estimated with atmospheric optical depths measured on the ground at the several wavelengths for aerosol scattering and absorption, and Rayleigh scattering derived from measured atmospheric pressure. Therefore, vicarious calibration coefficients are essentially absolute values.

Figure 1 shows flowchart of the vicarious calibration.

### C. Onboard Calibration

ASTER VNIR use lamp-based onboard calibrators for monitoring temporal changes in the sensor responses. Space restrictions aboard the Terra platform disallow a solar based calibration, and therefore, onboard calibration is lamp-based. VNIR has two onboard calibration lamps, lamp-A and lamp-B. Both are used periodically, and as a backup system.

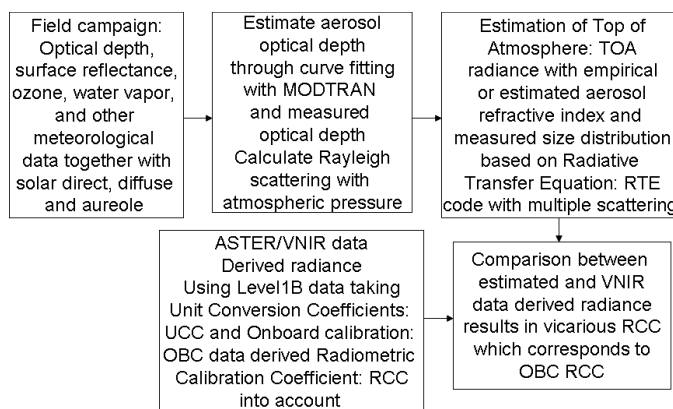


Fig. 1. Flowchart of the vicarious calibration

The VNIR calibration lamp output is monitored by a silicon photo monitor, and is guided to the calibration optics. The calibration optics output illuminates a portion of the VNIR aperture's observation optics and is monitored by a similar photo monitor. In the pre-flight phase, the onboard calibrators were well characterized with integration spheres calibrated with fixed freezing point blackbodies of Zn (419.5K). This was accomplished by comparing VNIR output derived from the integration sphere's illumination of the two sensors. The same comparison was made by the calibration lamp's (A and B) illumination of the two sensors. Next, the pre-flight gain and offset data (no illumination) were determined. In addition, MTF: Modulation Transfer Function was measured with slit light from a collimator while stray light effect was measured with the integration sphere illumination, which is blocked at the full aperture of the VNIR observation optics entrance. The pre-flight calibration data also includes (1) spectral response, (2) out-of-band response.

The VNIR has two onboard calibration halogen lamps (A and B). The light from these lamps is led to the VNIR optics via a set of calibration optics. Filters and photomonitors are located fore and aft of the calibration optics to monitor the output of the lamps as well as any possible degradation in the calibration optics. Lamp output and photo monitor data are collected every 33 days (primarily it was 16 days of the Terra orbital revisit cycle plus one day = 17 days and is 49 days now a day), and RCC: Radiometric Calibration Coefficients are calculated from the VNIR output taking into account the photo-monitor output. The RCC values are normalized by the pre-flight data to determine their final estimate. Thus, only data from a photo monitor that is aft of the calibration lamp is taken into account.

## III. EXPERIMENTS

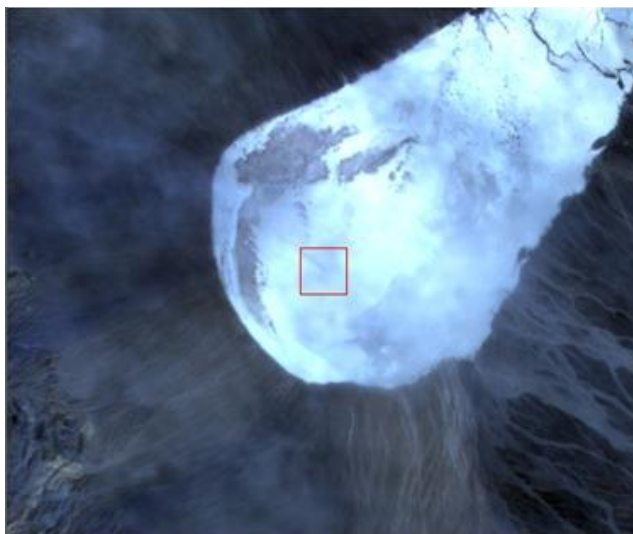
### A. Field Experiments Conducted

Field campaigns are conducted at the following three test sites,

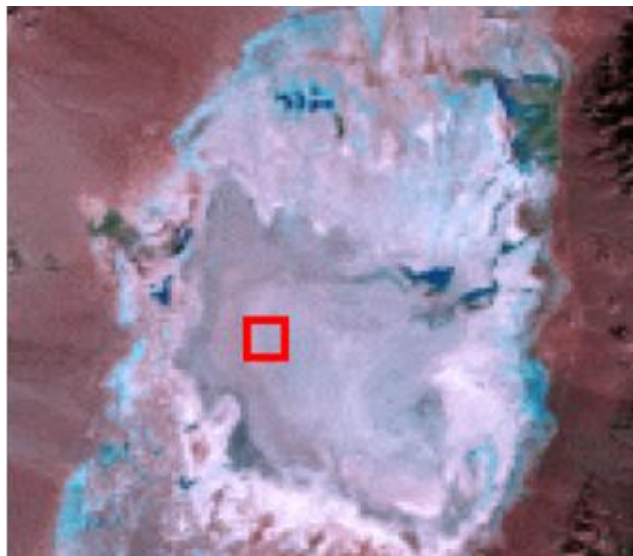
- IV: Ivanpah Playa (35:34N, 115:24W, 790m), California
- AL: Alkali Lake (37:51N, 117:25W, 1463m), Nevada
- RV: Railroad Valley Playa (38:30N, 115:41N, 1440m) Nevada



(a)Ivanpah Playa



(b)Alkali Lake



(c)Railroad Valley Playa

Fig. 2. Satellite view of three test sites

Figure 2 shows Terra/ASTER/VNIR observed three test-sites images. The red squares show the test-sites locations.

Table 2 shows the dates of the field campaigns. Target pixel can be identified through visual perception of blue tarp on the test sites. Thus the test site locations are precisely identified with good registration accuracy.

TABLE II. THE DATES OF THE FIELD CAMPAIGNS

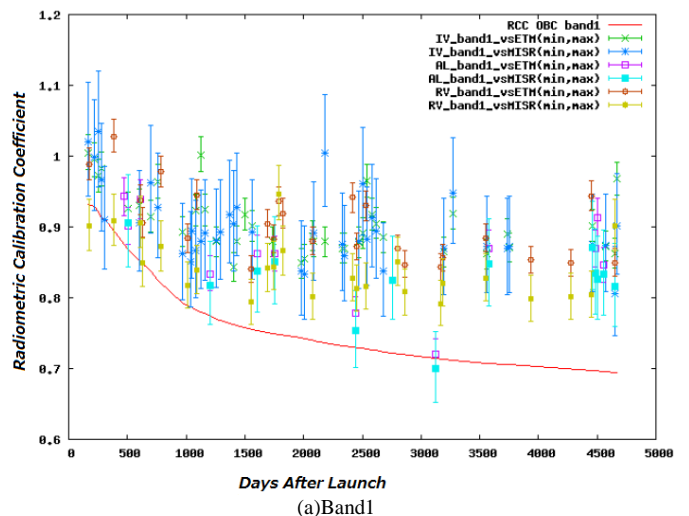
IV	AL	RV
0905 06/10/2002	2159 12/16/2005	2415 07/30/2006
2184 12/11/2005	2829 09/17/2007	3199 09/21/2008
2424 08/08/2006	3197 09/19/2008	3551 09/08/2009
2536 11/28/2006	3549 09/06/2009	3935 09/27/2010
2824 09/12/2007	3935 09/25/2010	4272 08/29/2011
3192 09/14/2008	4270 08/27/2011	4656 09/16/2012
3727 12/03/2008		
3544 09/01/2009		
3928 09/20/2010		
4265 08/22/2011		
4649 09/09/2012		

The first column shows the days after launch

### B. Radiometric Calibration Coefficient Comparisons

Figure 3 shows the Radiometric Calibration Coefficient: RCC of the onboard, vicarious and cross calibration. Red solid line in the figure shows RCC derived from Onboard Calibration: OBC data. OBC data derived RCC differs from both the conventional and the proposed cross calibration RCC.

These cross calibration coefficients are summarized with their averaged RCC and Standard Deviation: SD together with their Confidence Interval: CI at 95% of confidence level as shown in Table 3. As shown in Table 4, RMSD between the vicarious RCC and the proposed cross calibration RCC is less than that between the vicarious RCC and the cross calibration RCC.



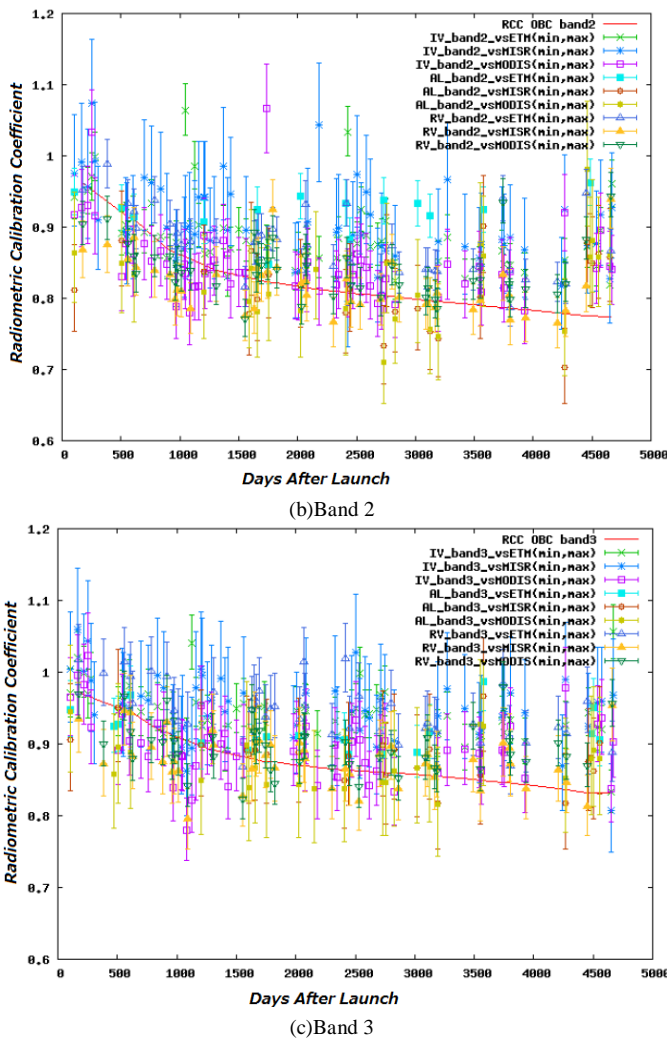


Fig. 3. Comparison of RCC among onboard, vicarious and cross calibration

TABLE III. SUMMARY OF CROSS CALIBRATION COEFFICIENTS

(a) Cross RCC for Green and Red bands						
		Green		Red		
		vsETM	vsMISR	vsETM	vsMISR	vsMODIS
IV	average (SD)	1.80 (0.54)	1.38 (0.45)	0.03 (0.15)	3.33 (0.90)	1.15 (1.33)
	95% CI	[1.38, 2.24]	[1.02, 1.74]	[-0.09, 0.15]	[2.61, 4.04]	[0.09, 2.21]
AL	average (SD)	1.41 (0.69)	1.46 (0.58)	-0.05 (0.16)	2.47 (1.02)	2.26 (0.72)
	95% CI	[0.52, 2.31]	[0.72, 2.21]	[-0.26, 0.15]	[1.16, 3.79]	[1.33, 3.19]
RV	average (SD)	0.88 (0.11)	2.34 (0.20)	-0.08 (0.12)	2.23 (0.28)	2.12 (0.29)
	95% CI	[0.74, 1.02]	[2.09, 2.60]	[-0.23, 0.07]	[1.87, 2.59]	[1.75, 2.50]

(b) Cross RCC for NIR band						
		NIR				
		vsETM	vsMISR	vsMODIS		
IV (N=11)	average (SD)	-1.81 (1.14)	-6.71 (1.83)	-5.09 (1.76)		
	95% CI	[-2.72, -0.90]	[-8.17, -5.25]	[-6.49, -3.69]		
AL (N=6)	average (SD)	-2.80 (0.97)	-8.94 (1.62)	-7.37 (1.41)		
	95% CI	[-4.06, -1.55]	[-11.04, -6.85]	[-9.19, -5.54]		
RV (N=6)	average (SD)	-2.67 (0.33)	-7.96 (1.37)	-6.65 (1.14)		
	95% CI	[-3.10, -2.24]	[-9.72, -6.19]	[-8.12, -5.18]		

Therefore, it is said that the proposed cross calibration method is superior to the conventional cross calibration

method obviously. Percent difference of RMSD between the conventional and the proposed cross calibration is shown in Table 5. It may be said that the proposed cross calibration method shows 6 to 89% better cross calibration accuracy in comparison to the conventional cross calibration.

TABLE IV. AVERAGED ROOT MEAN SQUARE DIFFERENCE BETWEEN VICARIOUS CALIBRATION RCC AND CROSS CALIBRATION RCC

Site	Conventional			Proposed		
	ETM+	MISR	MODIS	ETM+	MISR	MODIS
Ivanpah	0.0733	0.0798	0.0338	0.0690	0.0645	0.0169
Alkali	0.0280	0.0625	-	0.00312	0.0387	-
Railroad	0.0889	0.0194	0.0619	0.0807	0.0031	0.0346

TABLE V. PERCENT DIFFERENCE OF RMSD BETWEEN CONVENTIONAL AND PROPOSED CROSS RCC

Site	% Difference between Conventional and Proposed Cross RCC		
	ETM+	MISR	MODIS
Ivanpah		5.866	19.173
Alkali	88.857	38.080	-
Railroad	9.224	84.021	44.103

#### IV. CONCLUSION

Accuracy evaluation of cross calibration through band-to-band data comparison for visible and near infrared radiometers which onboard earth observation satellites is conducted. The conventional cross calibration for visible to near infrared radiometers onboard earth observation satellites is conducted through comparisons of band-to-band data of which spectral response functions are overlapped mostly.

There are the following major error sources due to observation time difference, spectral response function difference in conjunction of surface reflectance and atmospheric optical depth, observation area difference. These error sources are assessed with dataset acquired through ground measurements of surface reflectance and optical depth. Then the accuracy of the conventional cross calibration is evaluated with vicarious calibration data. The results show that cross calibration accuracy can be done more precisely if the influences due to the aforementioned three major error sources are taken into account.

#### ACKNOWLEDGMENT

The author would like to thank Ministry of Economy, Trade and Industry; METI for providing ASTER data and also thank Dr. Satoshi Tsuchida and his colleague of The National Institute of Advanced Industrial Science and Technology (AIST), and Dr. Fumihiro Sakuma and his colleague of The Japan Space Systems people for their support to this research works. The author also would like to thank Mr. Yuichi Sarusawa of Graduate School of Saga University for his efforts to conduct cross calibration experiments.

#### REFERENCES

[1] Arai, K., Calibration /intercalibration of multi-sensor for satellites, Advances in Space Research, Vol.16, No.10, pp.125-128, A31-002, July 1994.

- [2] P.Slater, K.Thome, A.Ono, F.Sakuma, Kohei Arai, F.Palluconi, H.Fujisada, Y.Yamaguchi and H.Kieffer, Radiometric Calibration of ASTER Data, Journal of Remote Sensing Society of Japan, Vol.15, No.2, pp.16-23, Jun.1994.
- [3] A.Ono, F.Sakuma, Kohei Arai, Y.Yamaguchi, H.Fujisada, P.Slater, K.Thome, F.Palluconi and H.Kieffer, Pre-flight and In-flight Calibration Plan for ASTER, Journal of Atmospheric and Oceanic Technology, Vol.13, No.2, pp.321-335, Apr.1995.
- [4] Kohei Arai, Inflight Test Site Cross Calibration Between Mission Instruments Onboard Same Platform, Advances in Space Research, Vol.19, No.9, pp.1317-1324, Jul.1997.
- [5] K.Thome, K.Arai et al., ASTER Preflight and Inflight Calibration and Validation of Level 2 Products, IEEE Trans.on Geoscience and Remote Sensing, Vol.36, No.4, 1161-1172, Sep.1998.
- [6] K.Thome, S.Schiller, J.Conel, K.Arai and S.Tasuchida, Results of the 1996 EOS vicarious calibration joint campaign at Lunar Lake Playa, Nevada(USA), Metrologia, Vol.35, pp.631-638, Jan.1999.
- [7] K.Arai, Error budget analysis of cross calibration method between ADEOS/AVNIR and OCTS, Advances in Space Research, Vol.23, No.8, pp.1385-1388, June 1999.
- [8] K.Arai, Preliminary vicarious calibration for EOS-AM1/ASTER with field campaign, Advances in Space Research, Vol.23, No.8, pp.1449-1457, June 1999.
- [9] Kohei Arai and H.Tonooka, Radiometric performance evaluation of ASTER/VNIR, SWIR and TIR, IEEE Trans. on GeoScience and Remote Sensing, 43,12,2725-2732, 2005.
- [10] Kohei Arai, Vicarious calibration for solar reflection channels of radiometers onboard satellites with deserted area of data, Advances in Space Research, 39, 1, 13-19, 2007.
- [11] Kurtis Thome, Kohei Arai, Satoshi Tsuchida and Stuart Biggar, Vicarious calibration of ASTER via the reflectance based approach, IEEE transaction of GeoScience and Remote Sensing, 46, 10, 3285-3295, 2008.
- [12] Chrysoulakis,Abrams, Feidas and Kohei Arai, Comparison of Atmospheric correction methods using ASTER data for the area of Crete, Greece, International Journal of Remote Sensing, 31,24,6347-6385,2010.
- [13] Ramachandran, Justice, Abrams(Edt.),Kohei Arai et al., Land Remote Sensing and Global Environmental Changes, Part-II, Sec.5: ASTER VNIR and SWIR Radiometric Calibration and Atmospheric Correction, 83-116, Springer 2010.
- [14] Arai, K., & Terayama, Y. (2000). An Experimental Study on Cross Calibration of ADEOS / AVNIR and the Visible Channels of OCTS. *Journal of Remote Sensing Society of Japan*, 20 (2), 60{68.
- [15] Cachorro, V. E., Frutos, A. M. D. E., Aplicada, D. D. F., Gonzalez, M. J., & Electrica, D. D. I. (1993). Analysis of the relationships between Junge size distribution and angstrom \_ turbidity parameters from spectral measurements of atmospheric aerosol extinction. *Atmospheric Environment*, 27A(10), 1585{1591.
- [16] Chandrasekhar, S. (1960). *Radiative transfer* (1st ed.). New York, US: Dover Publications, Inc.
- [17] Dinguirard, M., & Slater, P. (1999). Calibration of space-multispectral imaging sensors: A review. *Remote Sensing of Environment*, 4257 (98), 194{205. Earth Remote Sensing Data Analysis Center. (2005). *ASTER User's Guid Part I General* (Ver.4.0 ed.).
- [18] Liu, J.-J., Li, Z., Qiao, Y.-L., Liu, Y.-J., & Zhang, Y.-X. (2004, December). A new method for cross-calibration of two satellite sensors. *International Journal of Remote Sensing*, 25 (23), 5267{5281. Retrieved from <http://www.tandfonline.com/doi/abs/10.1080/01431160412331269779> doi: 10.1080/01431160412331269779
- [19] Teillet, P. M., Fedosejevs, G., Thome, K., & Barker, J. L. (2007, October). Impacts of spectral band difference effects on radiometric cross-calibration between satellite sensors in the solar-reflective spectral domain. *Remote Sensing of Environment*, 110 (3), 393{409. doi: 10.1016/j.rse.2007.03.003
- [20] Tsuchida, S., Sakuma, H., & Iwasaki, A. (2004). *Equations for ASTER radiometric calibration ver.0.20*. Retrieved 2013/01/24, from <http://staff.aist.go.jp/s.tsuchida/aster/cal/info/equation/index.html>
- [21] Xiong, X., Che, N., & Barnes, W. L. (2006). Terra MODIS On-Orbit Spectral Characterization and Performance. *IEEE transactions on Geoscience and Remote Sensing*, 44 (8), 2198{2206.
- [22] C.J. Brueggc and D.J. Diner, "Instrument verification tests on the Multi-angle imaging Spectro-Radiometer (MISR)," in *Earth Observing Systems II*, SPIE 3117, San Diego, CA, 28-29 July 1997.
- [23] P.M. Teillet, J.L. Barker, B.L. Markham, R.R. Irish, G. Fedosejevs, J.C. Storey, Radiometric cross-calibration of the Landsat-7 ETM+ and Landsat-5 TM sensors based on tandem data sets, *Remote Sensing of Environment* 78 (2001) 39– 54

#### AUTHORS PROFILE

**Kohei Arai**, He received BS, MS and PhD degrees in 1972, 1974 and 1982, respectively. He was with The Institute for Industrial Science and Technology of the University of Tokyo from April 1974 to December 1978 also was with National Space Development Agency of Japan from January, 1979 to March, 1990. During from 1985 to 1987, he was with Canada Centre for Remote Sensing as a Post Doctoral Fellow of National Science and Engineering Research Council of Canada. He moved to Saga University as a Professor in Department of Information Science on April 1990. He was a councilor for the Aeronautics and Space related to the Technology Committee of the Ministry of Science and Technology during from 1998 to 2000. He was a councilor of Saga University for 2002 and 2003. He also was an executive councilor for the Remote Sensing Society of Japan for 2003 to 2005. He is an Adjunct Professor of University of Arizona, USA since 1998. He also is Vice Chairman of the Commission "A" of ICSU/COSPAR since 2008. He wrote 30 books and published 442 journal papers

# Image Retrieval and Classification Method Based on Euclidian Distance Between Normalized Features Including Wavelet Descriptor

Kohei Arai<sup>1</sup>

Graduate School of Science and Engineering  
Saga University  
Saga City, Japan

**Abstract**—Image retrieval method based on Euclidian distance between normalized features with their mean and variance in feature space is proposed. Effectiveness of the normalization is evaluated together with a validation of the proposed image retrieval method. The proposed method is applied for discrimination and identifying dangerous red tide species based on wavelet utilized classification methods together with texture and color features. Through experiments, it is found that classification performance with the proposed wavelet derived shape information extracted from the microscopic view of the phytoplankton is effective for identifying dangerous red tide species among the other red tide species rather than the other conventional texture, color information. Moreover, it is also found that the proposed normalization of features is effective to improve identification performance.

**Keywords**—hue feature; texture information; wavelet descriptor; red tide; phytoplankton identification

## I. INTRODUCTION

The conventional image retrieval methods use the color information such as HSV<sup>1</sup>: Hue, Saturation and Value (Intensity), RGB: Red, Green, and Blue, etc. as the spectral information. Meanwhile texture information is also used in conventional image retrieval methods as the spatial information. On the other hand, Bachattarian [1], Euclidian<sup>2</sup>, Mahalanobis<sup>3</sup> distance measures [2] are well known as the similarity or distance measure. Not only hierarchical<sup>4</sup> and non-hierarchical clustering<sup>5</sup> as well as Bayesian rule of classification<sup>6</sup> and Maximum Likelihood classification<sup>7</sup>, but also Vector quantization<sup>8</sup>, Support vector machine<sup>9</sup>, etc. are proposed and used for image retrievals. Relational information such as the relations among image portions or segments,

semantic information, knowledge based information, relational similarity to classify semantic relations [3] etc. are tried to use in image retrievals. Spatial and spectral information derived from the images in concern is applicable image retrievals. There are some moment based spatial information extraction methods [4], [5], texture feature based spatial information extraction methods [6] and spectral information based image retrieval methods [7], [8], [9]. Furthermore, some attempts are made for image retrievals with wavelet descriptor as a spatial information extraction [9], [10]. In general, these conventional methods have not so good performance in terms of retrieval success rate.

Image retrieval method based on texture, hue and shape features is proposed [11]. In the proposed method, texture feature is extracted based on discrete wavelet transformation while shape feature is extracted by the proposed wavelet descriptor which allows extraction and representation of contour [12]. Contour of the object extracted from the original image can be expressed with wavelet based descriptor. The image retrieval method which is based on the hue information and texture as well as the wavelet described shape information of extracted objects is proposed previously to improve image retrieval success rate. Image retrieval performance is not good enough in particular for resemble red tide species. The method proposed here is normalization of features in concern with their mean and variance. Through the normalization, all the features used should have almost same influence for discrimination between the current specie and the referenced specie results in improvement of identification performance.

The following section describes the proposed image retrieval method followed by some experiments for reproducibility of the proposed wavelet descriptor in comparison to the conventional Fourier descriptor with several simple symmetrical and asymmetrical shapes. Then it is validated with the image database of phytoplankton [13].

## II. PROPOSED METHOD

### A. Process Flow of the Proposed Image Classification

Image classification method based on hue information [14] and wavelet description based shape information [15] as well as texture information of the objects extracted with dyadic wavelet transformation [16] is proposed. Object is assumed to be focused so that the frequency component in the object is

<sup>1</sup> [http://www.cs.rit.edu/~ncs/color/t\\_convert.html](http://www.cs.rit.edu/~ncs/color/t_convert.html)

<sup>2</sup> [http://en.wikipedia.org/wiki/Euclidean\\_distance](http://en.wikipedia.org/wiki/Euclidean_distance)

<sup>3</sup> [http://en.wikipedia.org/wiki/Mahalanobis\\_distance](http://en.wikipedia.org/wiki/Mahalanobis_distance)

<sup>4</sup> [http://en.wikipedia.org/wiki/Hierarchical\\_clustering](http://en.wikipedia.org/wiki/Hierarchical_clustering)

<sup>5</sup> <http://www.daylight.com/meetings/mug96/barnard/E-MUG95.html>

<sup>6</sup> [http://en.wikipedia.org/wiki/Naive\\_Bayes\\_classifier](http://en.wikipedia.org/wiki/Naive_Bayes_classifier)

<sup>7</sup> [http://www.ccrs.nrcan.gc.ca/glossary/index\\_e.php?id=341](http://www.ccrs.nrcan.gc.ca/glossary/index_e.php?id=341)

<sup>8</sup> [http://en.wikipedia.org/wiki/Learning\\_Vector\\_Quantization](http://en.wikipedia.org/wiki/Learning_Vector_Quantization)

<sup>9</sup> [http://en.wikipedia.org/wiki/Support\\_vector\\_machine](http://en.wikipedia.org/wiki/Support_vector_machine)

relatively high in comparison to the other (background). Figure 1 shows the process flow of the proposed image classification method.

One of the image features of hue information (angle) is calculated for the entire image in the color image database. Dyadic wavelet transformation<sup>10</sup> is also applied to the images then texture information is extracted from the transformed resultant image. Based on the Dyadic wavelet transformation, HH<sup>11</sup> image of edge is extracted from the original image. Morphological operations<sup>12</sup>, opening and closing are then applied to the edge extracted images to remove inappropriate isolated pixels and undesirable image defects. After that the resultant image is binarized with appropriate threshold then contour of the object is extracted. Then the Dyadic wavelet transformation is applied to the contour in order to extract shape information (Wavelet descriptor). After all, Euclidian distance between target image and the other candidate images in the color image database is calculated with extracted hue, texture and shape information then the closest image is retrieved.

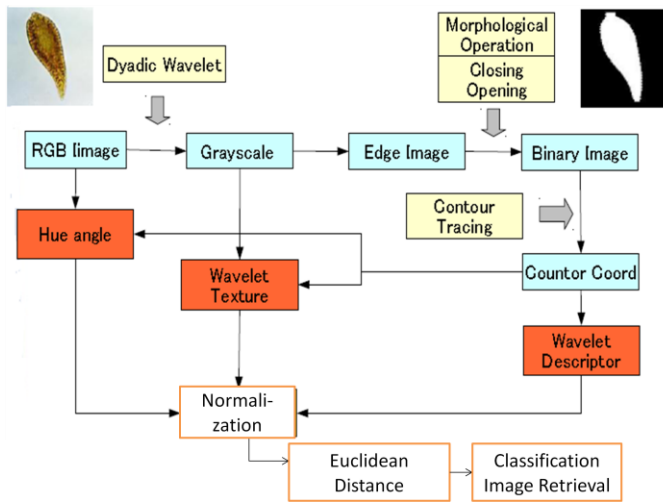


Fig. 1. Process flow of the proposed image classification method.

Normalization of the extracted features is applied in the proposed method. Then image in concern is retrieved with Euclidian distance between features of the image in concern and the images in the given image database.

### B. Dyadic wavelet transformation

Using dyadic wavelet, frequency component can be detected. Dyadic wavelet allows to separate frequency components keeping image size with that of original image. Dyadic wavelet is called as a binary wavelet and has high pass

and low pass filter components,  $\{h[k], g[k]\}$  and reconstruction filter  $\{\underline{h}[k], \underline{g}[k]\}$ . Low and high frequency components,  $C_n$  and  $d_n$  are expressed as follows,

$$C_n [i]=\sum_k h[k] C_{n-1} [i + k2^{n-1}] \quad (1)$$

$$d_n [i]=\sum_k g [k] C_{n-1} [i + k2^{n-1}] \quad (2)$$

Then original image is also reconstructed with the low and high frequency components as follows,

$$C_{n-1} [i]=1/2 \sum_k \underline{h}[k] C_n [i-k2^{n-1}]+\sum_k \underline{g}[k] d_n [i-k2^{n-1}] \quad (3)$$

If a new parameter  $s[m]$  is employed, then lifting dyadic wavelet is defined as follows,

$$h^{new}[k]=h^{old} [k] \quad (4)$$

$$\underline{h}^{new}[k]=\underline{h}^{old} [k] + \sum_m s[-m] \underline{g}^{old} [k-m] \quad (5)$$

$$g^{new}[k]=g^{old} [k] - \sum_m s[m] h^{old} [k-m] \quad (6)$$

$$\underline{g}^{new}[k]=\underline{g}^{old} [k] \quad (7)$$

### C. Dyadic wavelet based descriptor (Shape information)

Image classification method with hue and texture information is conventional. In the proposed method, another feature, shape information is employed. Fourier descriptor is used, in general, to represent shape information. Although Fourier descriptor represents frequency component of the contour line, location information cannot be described. In other words, Fourier descriptor does support only frequency analysis, and does not support time-frequency component analysis. Wavelet descriptor which is proposed by this paper supports a time-frequency component analysis so that not only frequency component but also location of contour edge can be discussed [17].

Let  $u(i)$  be distance between a point in the closed object contour line and a certain point  $i$  on the line, then the closed object contour line can be represented as  $u(i), i=1,2,\dots,n$ .  $i=1$  corresponds to 0 degree while  $i=n$  corresponds to 360 degree, respectively.  $u(i)$  can be converted with dyadic wavelet transformation. Then the contour line can be represented with high frequency component of the dyadic wavelet transformed sequence as is shown in Figure 2. Then average of the high frequency component of pixel value is used for a feature of the image classification.

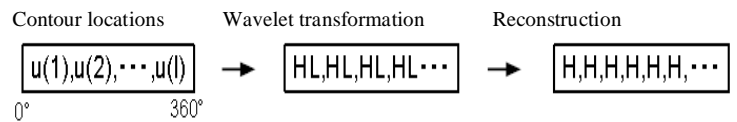


Fig. 2. Dyadic wavelet descriptor for representation of the closed object contour lines.

### D. Texture Feature

Also texture information is useful for discrimination. Texture information can be derived from dyadic wavelet transformation. Texture information is defined as high frequency component of pixel value derived from dyadic wavelet transformation. Daubechies wavelet transformation is applied to the 2x2 pixels defined in Figure 3.

<sup>10</sup>

[http://cas.ensmp.fr/~chaplais/Wavetour\\_presentation/ondelettes%20dyadiques/Dyadic\\_Transform.html](http://cas.ensmp.fr/~chaplais/Wavetour_presentation/ondelettes%20dyadiques/Dyadic_Transform.html)

<sup>11</sup> HH denotes high frequency component in horizontal direction and high frequency component in vertical direction

<sup>12</sup> [http://geol.hu/data/online\\_help/MorphologyFilters.html](http://geol.hu/data/online_help/MorphologyFilters.html)

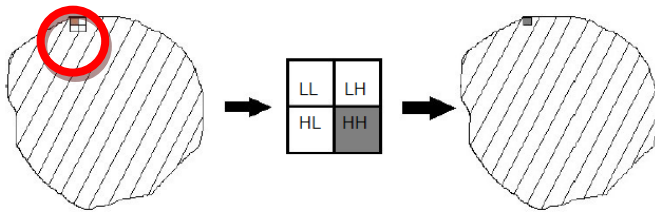


Fig. 3. Detected object and 2x2 of matrix in the object to detect texture information with 2x2 of dyadic wavelet transformation.

Pixel value of the pixel in the object is replaced to the high frequency component detected with Daubechies wavelet. Thus image which represents texture information of the detected object image is generated [18]. Daubechies base function of wavelet has order. 1 st order of Daubechies base function is totally equal to Haar base function. In this paper, 1st, 2nd, 4 th order of Daubechies base function is used and compare their classification and image retrieval performance with Euclidean distance between the specified phytoplankton and the others.

### E. Hue angle

Thus contour of the object is detected. Then Red, Green, and Blue: RGB of the original object image can be transformed to Hue, Saturation, and Intensity: HSV information. Hue information in unit of radian, in particular, is useful for discrimination of the target image classifications of phytoplankton images.

RGB to HSV conversion is also be expressed as follows,

$$\begin{aligned}
 V &= \max(R, G, B) \\
 S &= (V - X)/V \text{ where } X = \min(R, G, B) \\
 R = V: H &= (\pi/3) (b - g) \\
 G = V: H &= (\pi/3) (2 + r - b) \\
 B = V: H &= (\pi/3) (4 + g - r)
 \end{aligned}$$

where  $r = (V - R)/(V - X)$ ,  $g = (V - G)/(V - X)$ ,  $b = (V - B)/(V - X)$ ,  $H$  ranges from 0 to 360,  $S$  ranges from 0 to 1,  $V$  ranges from 0 to 1, HSV representation and R, G, B also range from 0 to 1.

These three features, hue,  $H$ , texture,  $xx$  and shape information,  $yy$  composes three dimensional feature space results in measurement of Euclidian distance between a query image and the images in previously created image database. Using the distance, a query image can be retrieved from the image in the database. Thus image classifications can be done with hue and texture information as well as shape information derived from dyadic wavelet descriptor.

## III. EXPERIMENTS

### A. Data Used

There are a plenty of red tide species. Small portion of red tide species can be listed up in Figure 1. These red tide species

can be classified into three categories, (a) Caution level of species, (b) Warning level of species, and (c) Dangerous species. Fishes and shells take these dangerous red tide species. After that human habitats eat the fishes and shells. Then such persons get a bad situation and have an illness condition. Therefore, these red tide species are classified into dangerous species.

Identifying these dangerous red tide species is important. It, however, is not so easy to classify because these three categories of red tide species are quite resemble. Usually, the local fishery research institutes measure red tide from the research vessels with microscope. They used to count the number of red tide with microscope camera acquired imagery data on the ship. Then identify the red tide species in the same time quickly. Even though human perception capability is superior to that by machine learning based automatic classification, there are some mistakes. The purpose of the research is to improve classification performance by using considerable features which can be extracted from the microscopic imagery data.

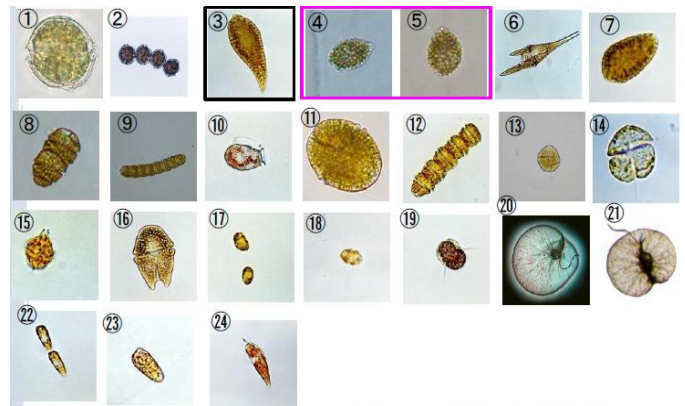


Fig. 4. Photos of a portion of red tide species

### B. Comparison of Euclidian Distance Between *Cahttnella Antiqua-3* and the Others with Three Features, Texture, Hue and Wavelet Descriptor Based on Daubechies 1, 2, and 4

One of the measures for classification performance evaluation is Euclidian distance among the classes in concern. Shorter Euclid distance implies a poor classification performance while longer distance means a good performance.

Euclid distance between *Chattnella Antiqua-3* and the other species are calculated and shown in Table 1, 2, 3 for the case of utilizing all these three features of wavelet descriptor with Daubechies 1, 2, and 4, respectively. Calculated Euclid Distance when Texture Wavelet Descriptor and hue information are used as features.

TABLE I. EUCLID DISTANCE BETWEEN CHATTNELLA ANTIQUA3 AND THE OTHERS WITH DAUBECHIES 1

Daubechies 1	Mean			Normalized Mean			Euclid Distance		
	wavelet	texture	hue(rad)	wavelet	texture	hue(rad)	Normalized	Mean	%Improve
a.catenella1cell	0.196484	4.320291	1.29206	4.320291	5.208882	3.47149	2.610026	0.730394	257.3451
a.catenella4cell	0.263178	5.48481	3.647233	5.48481	12.68603	5.002298	8.867848	3.258216	172.1688
c.antiqua	0.283669	5.571536	0.892777	5.571536	3.941248	5.472623	1.887694	1.870292	0.930425
c.antiqua2	0.288699	3.577128	2.054994	3.577128	7.631026	5.588075	3.60677	1.141521	215.9618
c.antiqua3	0.29426	3.701602	0.920312	3.701602	4.028665	5.715715	0	0	0
c.furca	0.246901	8.065513	1.742646	8.065513	6.639391	4.628697	5.200117	4.440745	17.1001
c.marina	0.222682	3.65	0.779962	3.65	3.583085	4.072805	1.703043	0.183073	830.2522
c.polykrikoides2cell	0.24923	3.70454	1.181714	3.70454	4.858558	4.682154	1.325511	0.271051	389.0264
c.polykrikoides8cell	0.217637	3.961787	1.173258	3.961787	4.831712	3.957009	1.950802	0.364634	435.0023
d.fortii	0.327144	9.655471	1.421595	9.655471	5.620126	6.470492	6.208945	5.975446	3.90763
g.catenatum1cell	0.210512	4.233059	0.83791	4.233059	3.767057	3.79347	2.011445	0.544842	269.1797
g.catenatum5cell	0.230301	8.044559	0.789282	8.044559	3.612674	4.247682	4.603199	4.345976	5.918657
g.instriatum	0.411956	4.286565	1.57805	4.286565	6.116836	8.417158	3.464165	0.896759	286.2983
g.mikimotoi	0.256012	5.721647	2.321516	5.721647	8.477174	4.837819	4.963921	2.459018	101.866
g.polygramma	0.295303	7.345761	1.019077	7.345761	4.342222	5.739655	3.657702	3.645502	0.334673
g.sanguineum	0.27297	9.884615	1.184978	9.884615	4.86892	5.227051	6.258951	6.188811	1.13334
h.akashiwo	0.550117	7.972222	0.993822	7.972222	4.262043	11.58833	7.265003	4.2888	69.39478
h.circularisquama	0.499699	4.288433	0.850071	4.288433	3.805666	10.4311	4.756989	0.665326	614.9864
m.rubrum	0.35107	7.850218	1.444111	7.850218	5.69161	7.019659	4.655821	4.182799	11.30874
n.scintillans4	0.225198	3.990742	2.205616	3.990742	8.109217	4.130554	4.387168	1.320164	232.3199
n.scintillans5	0.184937	2.872873	1.507892	2.872873	5.8941	3.206455	3.23466	1.026171	215.2166
Mean	0.289427	5.62778	1.420899	5.62778	5.617916	5.604776	3.934275	2.276169	196.6501
Standard Deviation	0.095136	2.183621	0.687803	2.183621	2.183621	2.183621	2.147732	1.994634	224.5983

TABLE II. EUCLID DISTANCE BETWEEN CHATTNELLA ANTIQUA3 AND THE OTHERS WITH DAUBECHIES 2

Daubechies 2	Mean			Normalized Mean			Euclid Disatance		
	wavelet	texture	hue(rad)	wavelet	texture	hue(rad)	Normalized	Mean	%Improve
a.catenella1cell	0.080995	4.320291	1.29206	4.320291	5.208882	3.705773	2.32756	0.730394	218.672
a.catenella4cell	0.170238	5.48481	3.647233	5.48481	12.68603	5.416414	8.841316	3.258216	171.3545
c.antiqua	0.155219	5.571536	0.892777	5.571536	3.941248	5.128525	1.933937	1.870292	3.402932
c.antiqua2	0.171255	3.577128	2.054994	3.577128	7.631026	5.435908	3.608915	1.141521	216.1497
c.antiqua3	0.180553	3.701602	0.920312	3.701602	4.028665	5.614136	0	0	0
c.furca	0.159615	8.065513	1.742646	8.065513	6.639391	5.212789	5.101048	4.440745	14.86918
c.marina	0.085888	3.65	0.779962	3.65	3.583085	3.799564	1.869191	0.183073	921.0066
c.polykrikoides2cell	0.117673	3.70454	1.181714	3.70454	4.858558	4.40883	1.463384	0.271051	439.8925
c.polykrikoides8cell	0.147278	3.961787	1.173258	3.961787	4.831712	4.976309	1.058019	0.364634	190.1588
d.fortii	0.236693	9.655471	1.421595	9.655471	5.620126	6.690247	6.256143	5.975446	4.697494
g.catenatum1cell	0.103167	4.233059	0.83791	4.233059	3.767057	4.130774	1.597262	0.544842	193.1609
g.catenatum5cell	0.098365	8.044559	0.789282	8.044559	3.612674	4.038728	4.63856	4.345976	6.732285
g.instriatum	0.315118	4.286565	1.57805	4.286565	6.116836	8.193524	3.369849	0.896759	275.781
g.mikimotoi	0.122712	5.721647	2.321516	5.721647	8.477174	4.505419	5.009897	2.459018	103.7357
g.polygramma	0.16845	7.345761	1.019077	7.345761	4.342222	5.382141	3.664974	3.645502	0.534143
g.sanguineum	0.134972	9.884615	1.184978	9.884615	4.86892	4.740423	6.300718	6.188811	1.808221
h.akashiwo	0.503999	7.972222	0.993822	7.972222	4.262043	11.81406	7.532047	4.2888	75.62133
h.circularisquama	0.429245	4.288433	0.850071	4.288433	3.805666	10.38115	4.808173	0.665326	622.6794
m.rubrum	0.260962	7.850218	1.444111	7.850218	5.69161	7.155443	4.727793	4.182799	13.02941
n.scintillans4	0.105809	3.990742	2.205616	3.990742	8.109217	4.181417	4.334419	1.320164	228.3243
n.scintillans5	0.053063	2.872873	1.507892	2.872873	5.8941	3.170363	3.184127	1.026171	210.2921
Mean	0.181013	5.62778	1.420899	5.62778	5.617916	5.622949	3.887016	2.276169	186.2811

Standard Deviation	0.113918	2.183621	0.687803	2.183621	2.183621	2.183621	2.233389	1.994634	233.1855
--------------------	----------	----------	----------	----------	----------	----------	----------	----------	----------

TABLE III. EUCLID DISTANCE BETWEEN CHATTNELLA ANTIQUA3 AND THE OTHERS WITH DAUBECHIES 4

Daubechies 4	Mean			Normalized Mean			Euclid Disatance		
	wavelet	texture	hue(rad)	wavelet	texture	hue(rad)	Normalized	Mean	%Improve
a.catenella1cell	0.088846	4.320291	1.29206	4.320291	5.208882	3.698761	2.237914	0.730394	206.3984
a.catenella4cell	0.194141	5.48481	3.647233	5.48481	12.68603	5.391889	8.839726	3.258216	171.3057
c.antiqua	0.176529	5.571536	0.892777	5.571536	3.941248	5.10869	1.911765	1.870292	2.217423
c.antiqua2	0.192126	3.577128	2.054994	3.577128	7.631026	5.359488	3.607122	1.141521	215.9926
c.antiqua3	0.200659	3.701602	0.920312	3.701602	4.028665	5.496697	0	0	0
c.furca	0.184336	8.065513	1.742646	8.065513	6.639391	5.234226	5.092004	4.440745	14.66552
c.marina	0.095042	3.65	0.779962	3.65	3.583085	3.798392	1.756543	0.183073	859.4753
c.polykrikoides2cell	0.129042	3.70454	1.181714	3.70454	4.858558	4.345107	1.419469	0.271051	423.6906
c.polykrikoides8cell	0.164878	3.961787	1.173258	3.961787	4.831712	4.921344	1.021573	0.364634	180.1637
d.fortii	0.278876	9.655471	1.421595	9.655471	5.620126	6.754414	6.289925	5.975446	5.26285
g.catenatum1cell	0.113391	4.233059	0.83791	4.233059	3.767057	4.093441	1.523159	0.544842	179.5599
g.catenatum5cell	0.105457	8.044559	0.789282	8.044559	3.612674	3.965864	4.623611	4.345976	6.388313
g.instriatum	0.372052	4.286565	1.57805	4.286565	6.116836	8.25267	3.506854	0.896759	291.0587
g.mikimotoi	0.147609	5.721647	2.321516	5.721647	8.477174	4.643661	4.959585	2.459018	101.6897
g.polygramma	0.194853	7.345761	1.019077	7.345761	4.342222	5.403337	3.658815	3.645502	0.365202
g.sanguineum	0.15963	9.884615	1.184978	9.884615	4.86892	4.836957	6.274626	6.188811	1.386621
h.akashiwo	0.588219	7.972222	0.993822	7.972222	4.262043	11.7286	7.558393	4.2888	76.23562
h.circularisquama	0.506198	4.288433	0.850071	4.288433	3.805666	10.40972	4.952965	0.665326	644.442
m.rubrum	0.302785	7.850218	1.444111	7.850218	5.69161	7.138867	4.76163	4.182799	13.83836
n.scintillans4	0.11566	3.990742	2.205616	3.990742	8.109217	4.129926	4.31307	1.320164	226.7071
n.scintillans5	0.0558	2.872873	1.507892	2.872873	5.8941	3.167387	3.097148	1.026171	201.8161
Mean	0.207911	5.62778	1.420899	5.62778	5.617916	5.613306	3.876471	2.276169	182.0314
Standard Deviation	0.135799	2.183621	0.687803	2.183621	2.183621	2.183621	2.255699	1.994634	225.2163

It is clear that the mean and standard deviation after the normalization are same in comparison to the before the normalization. It also found that the Euclidian distance between Chattrnella Antiqua-3 and the others are improved remarkably, around twice much longer distance.

C. Euclidian Distance Between Chattrnella-3 and the Others Using Hue and Texture information as well as with and without Wavelet Descriptor

Effectiveness of the wavelet descriptor is evaluated through comparisons of Euclidian distance between Chattrnella Antiqua-3 of specie and the other species calculated with the normalized features. Table 4, 5, 6 shows the results for Daubechies 1, 2, 4 of base function of wavelet.

The mean of Euclidian distance for without wavelet descriptor shows around 2.7 while that with wavelet descriptor shows more than 3.8. Therefore, effectiveness of wavelet descriptor is corresponding to 40% improvement of Euclidian distance which results in 40% improvement of image retrieval and classification.

TABLE IV. EUCLID DISTANCE BETWEEN CHATTNELLA ANTIQUA3 AND THE OTHERS WITH DAUBECHIES 1

Daubechies 1	With	Without
	Wavelet Descriptor	
a.catenella1cell	2.610026	2.535638

a.catenella4cell	8.867848	8.686708
c.antiqua	1.887694	0.258332
c.antiqua2	3.60677	3.604622
c.antiqua3	0	0
c.furca	5.200117	2.827985
c.marina	1.703043	1.702262
c.polykrikoides2cell	1.325511	1.325508
c.polykrikoides8cell	1.950802	1.933373
d.fortii	6.208945	1.761374
g.catenatum1cell	2.011445	1.939965
g.catenatum5cell	4.603199	1.525834
g.instriatum	3.464165	3.414419
g.mikimotoi	4.963921	4.534306
g.polygramma	3.657702	0.314469
g.sanguineum	6.258951	0.972019
h.akashiwo	7.265003	5.87725
h.circularisquama	4.756989	4.720654
m.rubrum	4.655821	2.11321
n.scintillans4	4.387168	4.37763
n.scintillans5	3.23466	3.126697
Mean	3.934275	2.740584
Standard Deviation	2.147732	2.077256

TABLE V. EUCLID DISTANCE BETWEEN CHATTNELLA ANTIQUA3 AND THE OTHERS WITH DAUBECHIES 2

Daubechies 2	With	Without
	Wavelet Descriptor	
a.catenella1cell	2.32756	2.243827
a.catenella4cell	8.841316	8.659621
c.antiqua	1.933937	0.493416
c.antiqua2	3.608915	3.606767
c.antiqua3	0	0
c.furca	5.101048	2.641396
c.marina	1.869191	1.868478
c.polykrikoides2cell	1.463384	1.463381
c.polykrikoides8cell	1.058019	1.025528
d.fortii	6.256143	1.921136
g.catenatum1cell	1.597262	1.506254
g.catenatum5cell	4.63856	1.629404
g.instriatum	3.369849	3.31869
g.mikimotoi	5.009897	4.584592
g.polygramma	3.664974	0.39005
g.sanguineum	6.300718	1.212189
h.akashiwo	7.532047	6.204316
h.circularisquama	4.808173	4.772227
m.rubrum	4.727793	2.26738
n.scintillans4	4.334419	4.324765
n.scintillans5	3.184127	3.07439
Mean	3.887016	2.724181
Standard Deviation	2.233389	2.096728

TABLE VI. EUCLID DISTANCE BETWEEN CHATTNELLA ANTIQUA3 AND THE OTHERS WITH DAUBECHIES 4

Daubechies 4	With	Without
	Wavelet Descriptor	
a.catenella1cell	2.237914	2.150694
a.catenella4cell	8.839726	8.657998
c.antiqua	1.911765	0.397732
c.antiqua2	3.607122	3.604973
c.antiqua3	0	0
c.furca	5.092004	2.623887
c.marina	1.756543	1.755785
c.polykrikoides2cell	1.419469	1.419465
c.polykrikoides8cell	1.021573	0.987884
d.fortii	6.289925	2.028448
g.catenatum1cell	1.523159	1.427433
g.catenatum5cell	4.623611	1.586348
g.instriatum	3.506854	3.457722
g.mikimotoi	4.959585	4.529559
g.polygramma	3.658815	0.32716
g.sanguineum	6.274626	1.06831
h.akashiwo	7.558393	6.236273
h.circularisquama	4.952965	4.918078
m.rubrum	4.76163	2.337115
n.scintillans4	4.31307	4.303367
n.scintillans5	3.097148	2.984214

Mean	3.876471	2.704878
Standard Deviation	2.255699	2.126147

#### IV. CONCLUSION

Comparative study on discrimination methods for identifying dangerous red tide species based on wavelet utilized classification methods is conducted. Through experiments, it is found that classification performance with the proposed wavelet derived shape information extracted from the microscopic view of the phytoplankton is effective for identifying dangerous red tide species among the other red tide species rather than the other conventional texture, color information.

It is clear that the proposed wavelet descriptor is effective for image retrieval and classification. It is almost 40 % improvement in terms of Euclidian distance.

Normalization of features is effective to improve Euclidian distance between specie in concern and the others. The experimental results show that the Euclidian distance between *Chattnella Antiqua-3* and the others are improved remarkably, around twice much longer distance.

#### ACKNOWLEDGMENT

The author would like to thank Mr. Yuji Yamada for his effort to conduct the experiments.

#### REFERENCES

- [1] Duda R.O., P.E. Hart, and D.G. Stork, (2001), Pattern Classification, (Second Edition), John Wiley & Sons Inc.
- [2] Arai K. (1996), Fundamental theory for image processing, Gakujutsu-Tosho Shuppan Publishing Co., Ltd.
- [3] Séaghdha, D.O., Ann Copestake, (2009), Using lexical and relational similarity to classify semantic relations, Computational Linguistics 621-629.
- [4] Teh C.H. and R. T. Chin,(1988), On image analysis by the methods of moments, IEEE Trans. On Pattern Analysis and Machine Intelligence, 10, 4, 496-513
- [5] Taubin G. and D. B. Cooper,(1991), Recognition and Positioning of Rigid Objects Using Algebraic Moment Invariants, SPIE Conf. On Geometric Methods in Computer Vision, 1570, 175-186.
- [6] Niblack W.,(1993), The QBIC Project: Querying Images By Content Using Color, Texture and Shape, SPIE Conf. On Storage and Retrieval for Image and Video Databases, 1908, 173-187.
- [7] Zahn C.T., and Ralph Z. Roskies. (1972), Fourier Descriptors for Plane closed Curves. IEEE Trans. On Computer,c-21(3):269-281.
- [8] Huang C.L. and D.H. Huang,(1998), A Content-based image retrieval system. Image and Vision Computing, 16:149-163.
- [9] Yang H.S., S.U. Lee, K M. Lee., (1998), Recognition of 2D Object Contours Using Starting-Point-Independent Wavelet Coefficient Matching. Journal of Visual Communication and Image Representation, 9, 2, 171-181.
- [10] Tieng Q.M. and W. W. Boles, (1997), Recognition of 2D Object Contours Using the Wavelet Transform Zero-Crossing Representation, IEEE Trans. on PAMI 19, 8, 1997.
- [11] Grandlund H., (1972), Fourier preprocessing for hand print character recognition, IEEE Trans. on Computers, 621, 195-201.
- [12] Gibbs, J. W., (1899), "Fourier Series". Nature 59, 200 and 606.
- [13] Arai K. and Yasunori Terayama (2010), Polarized radiance from red tide, Proceedings of the SPIE Asia Pacific Remote Sensing, AE10-AE101-14.
- [14] Arai K. et al. (1991), Takagi and Shimoda ed., Image Analysis Handbook, Tokyo Daigaku Shuppan-kai publishing.

- [15] Arai K. (1998), Methods for Image Processing and Analysis of Earth Observation Satellite Imagery Data, Morikita Shuppan Publishing Co., Ltd.
- [16] Arai K. and L. Jameson (2001), Earth observation satellite data analysis based on wavelet analysis, Morikita-Shuppan Publishing Co., Ltd.
- [17] Arai K. (2002), Java based Earth observation satellite imagery data processing and analysis, Morikita-Shuppan Publishing Co., Ltd.
- [18] Arai, K., (2011), Visualization of 3D object shape complexity with wavelet descriptor and its application to image retrievals, Journal of Visualization, 15, 155-166.

AUTHORS PROFILE

**Kohei Arai**, He received BS, MS and PhD degrees in 1972, 1974 and 1982, respectively. He was with The Institute for Industrial Science, and

Technology of the University of Tokyo from 1974 to 1978 also was with National Space Development Agency of Japan (current JAXA) from 1979 to 1990. During from 1985 to 1987, he was with Canada Centre for Remote Sensing as a Post Doctoral Fellow of National Science and Engineering Research Council of Canada. He was appointed professor at Department of Information Science, Saga University in 1990. He was appointed councilor for the Aeronautics and Space related to the Technology Committee of the Ministry of Science and Technology during from 1998 to 2000. He was also appointed councilor of Saga University from 2002 and 2003 followed by an executive councilor of the Remote Sensing Society of Japan for 2003 to 2005. He is an adjunct professor of University of Arizona, USA since 1998. He also was appointed vice chairman of the Commission "A" of ICSU/COSPAR in 2008. He wrote 30 books and published 332 journal papers

# Numerical Representation of Web Sites of Remote Sensing Satellite Data Providers and Its Application to Knowledge Based Information Retrievals with Natural Language

Kohei Arai<sup>1</sup>

Graduate School of Science and Engineering  
Saga University  
Saga City, Japan

**Abstract**—A method for numerical expression of web site which is relating to satellite remote sensing and its application to knowledge based information retrieval system which allows retrievals with natural language is proposed and implemented. Through experiments with remote sensing related information, it is found that the proposed information retrieval system does work in particular for remote sensing satellite data retrievals with natural language.

**Keywords**—Information retrieval; Knowledge based system; Natural language; Feature mapping

## I. INTRODUCTION

When a word or words are typed in search engines, a list of web sites that contain those words is displayed. The words you enter are known as a query [1]. Baeza-Yates and Ribeiro-Neto linked Information Retrieval to the user information needs which can be expressed as a query submitted to a search engine [2]. Search engines were also known as some of the brightest stars in the Internet investing frenzy that occurred in the late 1990s [3]. Although search engines are programmed to rank websites based on their popularity and relevancy, empirical studies indicate various political, economic, and social biases in the information they provide [4],[5].

There are great amount of information for remote sensing satellite data retrievals. Directory, inventory, catalog, and guide information are available in a worldwide basis. Smart search engine, therefore, is needed for remote sensing satellite data retrievals. In order to realize a smart search engine, knowledge base system has to be involved. Knowledge base system consists of knowledge base which includes object and attribute, and inference engine. Also, users would like to search remote sensing satellite data with natural language.

The next section describes the proposed knowledge based search engine which allows search appropriate URLs of remote sensing satellite data providers with natural language followed by some experimental results. Then conclusion is described together with some discussions.

## II. PROPOSED INFORMATION RETRIEVAL SYSTEM

### A. Knowledge Based System and Conventional Information Retrieval Systems

Figure 1 shows configuration of knowledge based system which consists of Inference Engine: IE, Knowledge Base database: KB, Knowledge Base Management System: KBMS and Knowledge Acquisition Module: KAM. When user submits query to the knowledge based system, previously acquired knowledge about remote sensing satellite data providers is used to output search results. Also Figure 2 shows the query system which allows distribution of multiple queries to the multiple databases which include different types of remote sensing satellite data through expanded query generator from a single query. Therefore, appropriate queries are submitted from expanded query generator by database system by database system.

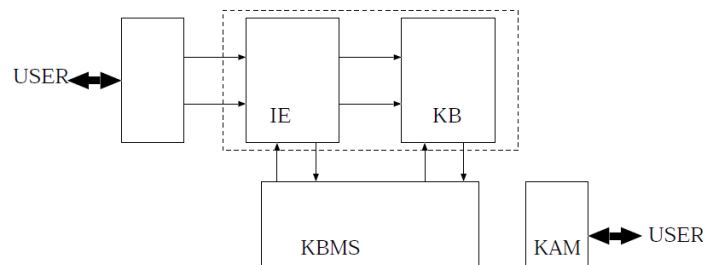


Fig. 1. Fundamental configuration of knowledge based system

There are distributed remote sensing satellite database systems created and managed by the data providers. Figure 3 shows assisted search module which allows distributed database servers search through internet. Only thing users have to do is to access the assisted search module. Then the module makes a search for appropriate database server from the distributed servers.

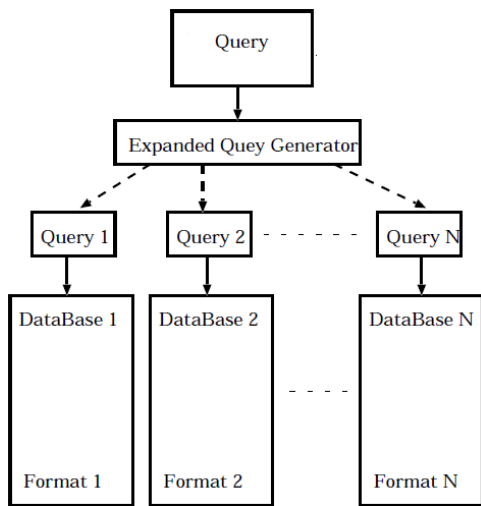


Fig. 2. Expanded query generator

There is NOAA: National Oceanic and Atmospheric Administration, EOSDIS: Earth Observation Satellite System of Data Information System, USGS: United States Geological Survey, DOE: Department of Energy, etc. as database servers of data providers. This assisted search module is the fundamental function of GCDIS-ASK: Global Change Data and Information System of Assisted Search for Knowledge.

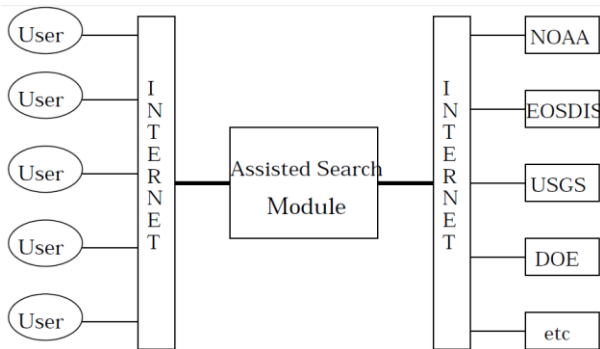


Fig. 3. Assisted search module

There are three basic components for GCDIS-ASK, client module, assisted search module and data collection module. Figure 4 shows system architecture of client module.

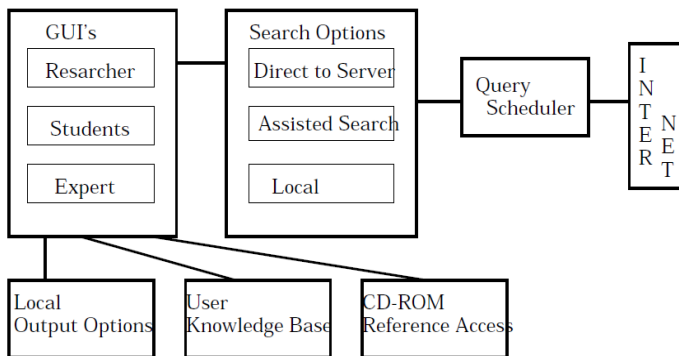


Fig. 4. Client module of GCDIS-ASK

When query is submitted from users, there are three options, direct search for the database, assisted search, and local search for the database under the GUI: Graphical User Interface.

One of the key features of assisted search module is Natural Language: NL search engine. Search can be done with a combination of statistical search and concept base search. The former is based on statistical variables, frequency of the query words, distance between query words, etc. On the other hands, the later uses concepts derived from expertise persons. Thus users can create concepts by using previously acquired knowledge and expertise in the knowledge base in order to improve search performance. Extendable knowledge base system makes such data and information search available. Under the extendable knowledge base system, there is NL search engine which consists of dictionary.

In order for that, smart query server and smart query scheduler are prepared as shown in Figure 5. There is specific database server under each smart query server. Search query scheduler monitors each smart query server. When user submits a query, client handler makes query generation and send query to appropriate smart query servers as shown in Figure 6.

Figure 7 shows more detailed architecture of assisted search module. Key issues here are NL search engine and user profiling. Users may use natural language in their queries. Users' profiles are archived and used for choosing information access options. Therefore, every time user access to the database, user profile is updated and thus information and data search can be done in much efficient way.

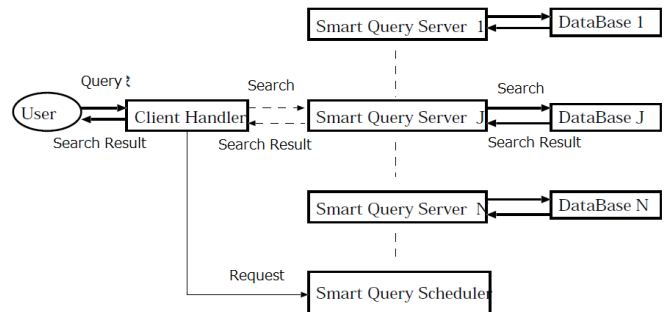


Fig. 6. Smart query scheduler and smart query servers

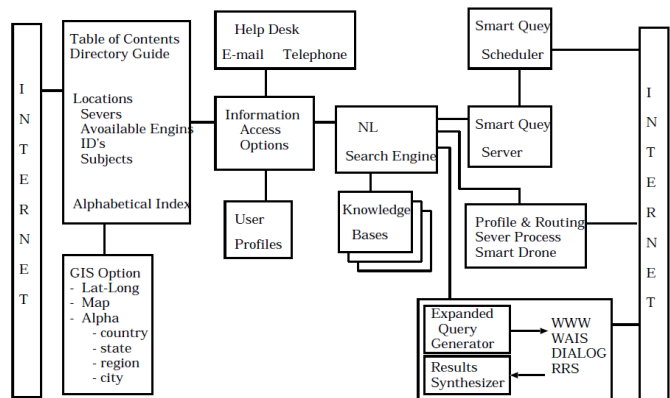


Fig. 7. Detailed architecture of assisted search module

Architecture of Data Collection Module: DCM is shown in Figure 8. Database search methods are different by data providers. User, however, can retrieve data and information from the different database servers in a unified way through this DCM.

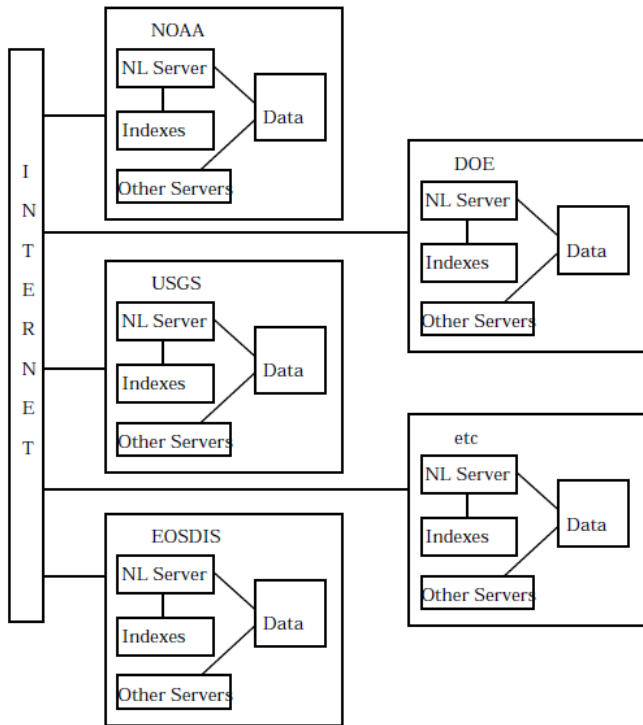


Fig. 8. Data Collection Module

**B. Proposed Information Retrieval Systems**

There are attribute information about data provider, keywords about URL, URL itself, data provider name, available data period (from when to when), information about data provider. There are attribute information about data, atmosphere, hydrosphere, cryosphere, geosphere, biosphere. Under the attribute information, there are many sensor names as shown in Table 1.

In the attribute information about data, there are observation target names, satellite names, sensor names, etc. as shown in Table 2. This is the example of NSIDC: National Snow and Ice Data Center.

Then it becomes possible to plot all URL in the five dimensional (attributes) vector space as shown in Figure 9. In the figure, x, y, and z axis are hydrosphere, cryosphere, and geosphere, respectively. Then the distance between URLs can be defined as shown in Figure 10. Angle between URLs can be calculated easily. Thus the smallest angle between input search query and the existing URL can be found followed by sending the closest URL to users as search result.

These attribute information can be classified as shown in Table 3. In the Table 3, number denotes the number of attribute and can be normalized as shown in the bottom row of the Table 3.

TABLE II. A VARIETY OF ATTRIBUTE INFORMATION ABOUT DATA WHICH ARE PROVIDED BY NSIDC

Attribution
snow
vegetation
river
sea ice
ice sheet
elevation
water vapor
avalanche
glacier
permafrost
RADARSAT
NOAA
AVHRR
SSM/I
LAI
snowstorm
SST

TABLE III. CLASSIFIED ATTRIBUTE INFORMATION AND THE NUMBER OF ATTRIBUTES

Feature	Atmosphere	Hydrosphere	Cryosphere	Geosphere	Biosphere
Attribute	water vapor NOAA	river sea ice NOAA AVHRR SSM/I SST	snow sea ice ice sheet avalanche glacier permafrost RADARSAT snowstorm	elevation NOAA RADARSAT	vegetation LAI
Number	2	6	8	3	2
	↓ Normalization ↓				
	(0.184900, 0.554700, 0.739600, 0.277350, 0.184900)				

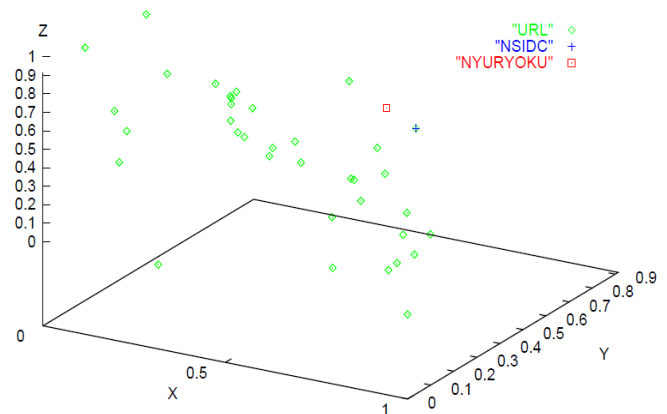


Fig. 9. URL distribution in the feature space of attributes (Hydrosphere, Cryosphere, and Geosphere)

TABLE I. SENSOR NAMES UNDER THE ATTRIBUTION INFORMATION

Atmosphere	Hydrosphere	Cryosphere	Geosphere	Biosphere
volcanic smoke	sea wind	snow	wild fire	vegetation
volcanic ash	river	ice	forest fire	oilfire
cyclone	rain	snow covered area	LST	NPP
ozone	sea ice	glacial landforms	volcanic eruption	desertification
sea wind	sea	ice sheet	land	acid rain
cloud	ocean color	ENVISAT	earthquake	tree crown
hurricane	SST	X-SAR	elevation	vegetation index
storm	El Nino	RADARSAT	liquefaction	tropical rain forest
water vapor	oil slick	sea ice	fire burn area	NDVI
air	chlorophyll	avalanche	carbonatite	vegetation cover rate
humidity	flood	glacier	crater temperature	vegetation community
aerosol	acid rain	permafrost	volcanic landforms	biomass
El Nino	ASTER	atmospheric ice	igneous rock	LAI
ozone layer	AMI	MSR	drought	red edge
total ozone	ALMAZ	ADEOS-2	desertification	HIRS/2
global warming	EOS	ILAS-2	iron oxide	PRIRODA
fumaric gas	AVHRR	MISR	SPOT	OKEAN
UV	PR	MOPITT	X-SAR	VCL
AMI	OCTS	RA	JERS-1	disaster
EOS	MOS-1	ATSR-M	sedimentary rock	environment
atmosphere	GOES	ATSR-2	fault	resource of agriculture
albedo	SEASAT	MERIS	TM	
HCMM	SeaStar	AATSR	stratum	
GOME	DMSP	IRS-1C/1D	mud flow	
greenhouse effect	TOPEX/POSEIDON	WiFS	debris flow	
GOES	NIMBUS	PAN	lava	
GMS	CZCS	disaster	ophiolite	
DMSP	TRMM	snow cover	ASTER	
NINBUS	NOAA	NOAA	ETM+	

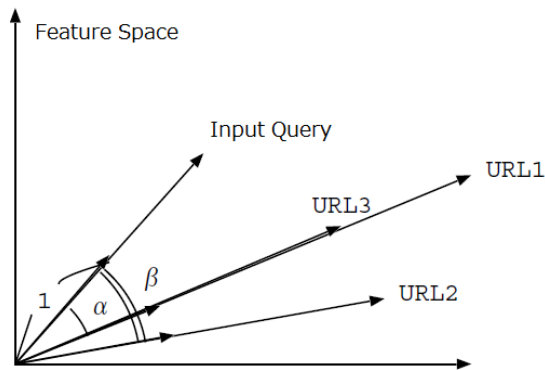


Fig. 10. Relation between input query and the existing URLs

Figure 11 shows architecture of the proposed remote sensing satellite data and information retrieval system.

Query from users is written in text format with natural language. Then angle between URLs can be calculated easily. Thus the smallest angle between input search query and the existing URL can be found followed by sending the closest URL to users as search result.

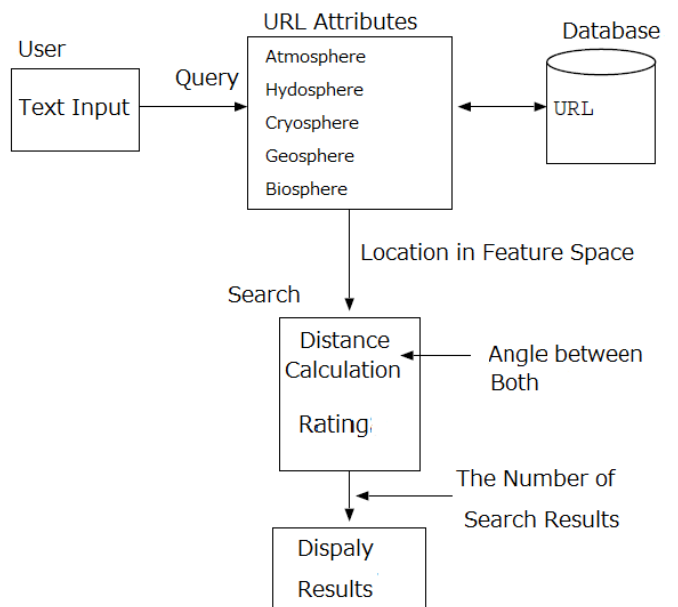


Fig. 11. Architecture of the proposed remote sensing satellite data and information retrieval system

### III. IMPLEMENTATION AND EXPERIMENTS

#### A. Implementation

Using netscape environment, web design is performed with PHP. Top page of the proposed search system is shown in Figure 12.

#### B. Search Example

In the example of Figure 12, search request is done with the following natural language,

“I would like to get images of areas suffered from heavy snow. I would like to know situation of iceberg in the Antarctic Ocean using data from Polar 1km AVHRR dataset. I would like to know about icy content mapped from space with RADARSAT.”



Fig. 12. Query input web page

When users submit the query together with users ID and the maximum number of search results, then the search result is returned as shown in Figure 13. For the example, the top five closest data providers to the query are output as search result with URL and the detailed information. These are aligned in accordance with the distance (angle) between query and the attribute information about data provider of URLs.

Users can refine the search results by reselecting much appropriate wording for query as shown in Figure 14. Then users can get much suitable URLs. Users' satisfaction is evaluated through questionnaire with the ten students and compares the evaluation result to the conventional keyword

search. As the result, all students prefer the proposed natural language search rather than the conventional keyword search. Hit ratio is also evaluated with ten students and compare to the keyword search. It is found that approximately 10 points improvement is confirmed for the proposed search system in comparison to the conventional keyword search.

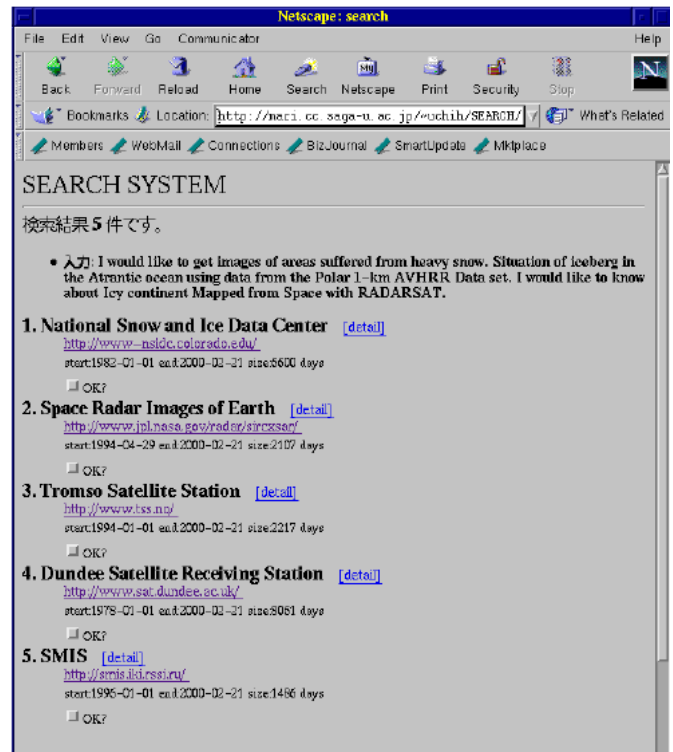


Fig. 13. Search result for the query of with the following natural language, “I would like to get images of areas suffered from heavy snow. I would like to know situation of iceberg in the Antarctic Ocean using data from Polar 1km AVHRR dataset. I would like to know about icy content mapped from space with RADARSAT.”

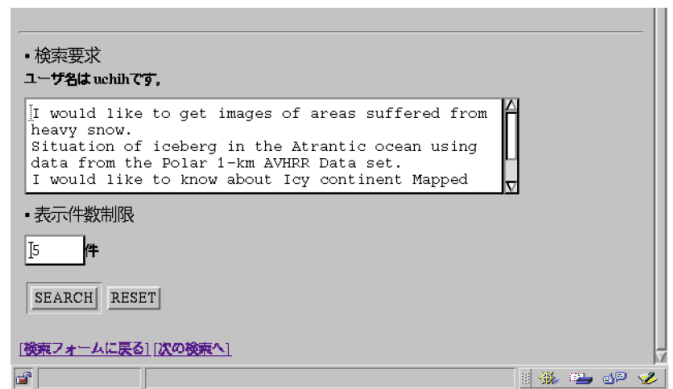


Fig. 14. Refinement of the search result by submit query with modified natural language again.

### IV. CONCLUSION

A method for numerical expression of web site which is relating to satellite remote sensing and its application to knowledge based information retrieval system which allows retrievals with natural language is proposed and implemented.

Through experiments with remote sensing related information, it is found that the proposed information retrieval system does work in particular for remote sensing satellite data retrievals with natural language

Users' satisfaction is evaluated through questionnaire with the ten students and compares the evaluation result to the conventional keyword search. As the result, all students prefer the proposed natural language search rather than the conventional keyword search. Hit ratio is also evaluated with ten students and compare to the keyword search. It is found that approximately 10 points improvement is confirmed for the proposed search system in comparison to the conventional keyword search.

#### ACKNOWLEDGMENT

The author would like to thank Mr. Fumihito Uchihashi for his effort to implement the proposed search engine and to conduct experiments with ten students.

#### REFERENCES

- [1] S. Brin and L. Page. The anatomy of a large-scale hypertextual Web search engine. In WWW, 1998.

- [2] Ricardo Baeza-Yates and Berthier Ribeiro-Neto. *Modern Information Retrieval*. Addison Wesley, May 1999.
- [3] Gandal, Neil (2001). "The dynamics of competition in the internet search engine market". *International Journal of Industrial Organization* **19** (7): 1103–1117
- [4] Segev, Elad (2010). *Google and the Digital Divide: The Biases of Online Knowledge*, Oxford: Chandos Publishing
- [5] Vaughan, L. & Thelwall, M. (2004). Search engine coverage bias: evidence and possible causes, *Information Processing & Management*, 40(4), 693-707

#### AUTHORS PROFILE

**Kohei Arai**, He received BS, MS and PhD degrees in 1972, 1974 and 1982, respectively. He was with The Institute for Industrial Science and Technology of the University of Tokyo from April 1974 to December 1978 also was with National Space Development Agency of Japan from January, 1979 to March, 1990. During from 1985 to 1987, he was with Canada Centre for Remote Sensing as a Post Doctoral Fellow of National Science and Engineering Research Council of Canada. He moved to Saga University as a Professor in Department of Information Science on April 1990. He was a councilor for the Aeronautics and Space related to the Technology Committee of the Ministry of Science and Technology during from 1998 to 2000. He was a councilor of Saga University for 2002 and 2003. He also was an executive councilor for the Remote Sensing Society of Japan for 2003 to 2005. He is an Adjunct Professor of University of Arizona, USA since 1998. He also is Vice Chairman of the Commission "A" of ICSU/COSPAR since 2008. He wrote 30 books and published 322 journal papers